REPORT DOCUMENTATION PAGE

Form Approved
OMB No. 0704-0188

1. AGENCY USE ONLY (Leave Blank)	2. REPORT DATE	3. REPORT TYPE AND DATES COVERED
	90-08-28	Final Technical, 86-11-01 to 90-03-31

4. TITLE AND SUBTITLE
Ultrafast Optical Electronics Center

5. FUNDING NUMBERS
AF 49620-87-C-0016

6. AUTHOR(S)
Mourou, Gerard

7. PERFORMING ORGANIZATION NAME(S) AND ADDRESS(ES)
University of Rochester
Laboratory for Laser Energetics
250 East River Road
Rochester, NY 14623-1299

8. PERFORMING ORGANIZATION REPORT NUMBER
n/a
AFOSR-TR- 90 0916

9. SPONSORING/MONITORING AGENCY NAME(S) AND ADDRESS(ES)
AFOSR
Building 410
Bolling AFB, DC 20332-6448
Technical Monitor: Dr. G. Witt

10. SPONSORING/MONITORING AGENCY REPORT NUMBER
3484/A3

900904

11. SUPPLEMENTARY NOTES

12a. DISTRIBUTION/AVAILABILITY STATEMENT
Unlimited

12b. DISTRIBUTION CODE

13. ABSTRACT (Maximum 200 words)

The work done under the URI had the mission to bridge ultrafast optics with high-speed electronics and photonics. Ultrashort optical pulses have been used to study fundamental processes taking place in the femtosecond and picosecond timescales in bulk and layered semiconductors, metals, and superconductors. Under this contract electron velocity overshoot in GaAs was time-resolved for the first time. Using short optical and electrical pulses, both sequential and resonant tunneling transport were investigated. The high-frequency properties of high-Tc superconductors in the 10-100 GHz range were studied. Time-resolved thermo-modulation was used to investigate the electron phonon interaction in metals. This URI also had an important technological impact. Novel techniques and devices were demonstrated. In particular, time-domain reflectometry, based on electro-optic sampling to test devices and circuits at room and cryogenic temperatures was developed. We tested HEMT, PBT, heterostructure transistor prescaler, NMOS silicon multiplexer, and GaAs power amplifier MMIC. Broadband electronics requires a complete understanding of normal and superconducting transmission lines. Extensive work has been done in this area. A time-resolved high-reflection, high-energy electron diffraction technique was also demonstrated and used to determine the surface temperature of the first monolayers in crystals. Ultrafast photoconductive detectors based on cold-grown GaAs with 0.5 ps temporal resolution were demonstrated. Also a velocity-matched, ultrahigh bandwidth (> 100 GHz), optical modulator and superconducting gate MODFET were shown. Finally because the work done under this URI hinged around our capability to generate, manipulate, and amplify optical pulses, it was necessary to perfect and develop new laser techniques. A good example has been the development of the chirped pulse amplification.

14. SUBJECT TERMS	15. NUMBER OF PAGES
ultrafast optics, high-speed electronics, electron transport in solids, velocity overshoot, resonant tunneling time-resolved RHEED, fast modulators, fast detectors, high-peak-power laser.	72
	16. PRICE CODE n/a

17. SECURITY CLASSIFICATION OF REPORT	18. SECURITY CLASSIFICATION OF THIS PAGE	19. SECURITY CLASSIFICATION OF ABSTRACT	20. LIMITATION OF ABSTRACT
unclassified	unclassified	unclassified	UL

Ultrafast Optical Electronics Center

Final Technical Report

For November 1, 1986 - March 31, 1990

Air Force Office of Scientific Research
University Research Initiative

Contract No. ~~AFOSR C~~F 49620-87-C-0016

University of Rochester
Laboratory for Laser Energetics
250 East River Road
Rochester, NY 14623-1299

Table of Contents

Introduction

Research using ultrashort optical pulses is making an enormous impact in the field of high-speed electronics and photonics critical to the next generation of fast communication and computer systems. Ultrashort pulses are playing an important role in the study of transient physical processes in solids, *i.e.*, semiconductors, metals, and superconductors. They also make possible the generation and detection of electrical signals with bandwidth over one order of magnitude higher than that attainable using convention purely electronic systems. Under this URI we looked at some of the fundamental issues involved in Boltzmann and quantum mechanical transport. Velocity overshoot was directly time-resolved. Sequential and resonant tunneling were experimentally studied. Electron-phonon relaxation in metals was studied and the frequency response of high-temperature superconductors was measured. In surface physics a novel reflection, high-energy-electron diffraction (RHEED) technique was developed and used to time-resolve the surface temperature of crystals by means of the Debye-Waller effect. This URI was also important in promoting the role of ultrafast optics in high-speed technology. Short electrical pulses in conjunction with the electro-optic effect were used to characterize devices and circuits up to 100 GHz. Ultrafast photoconductive detectors based on cold-grown GaAs with 0.5-ps temporal resolution were demonstrated. Also a velocity-matched, ultrahigh bandwidth (> 100 GHz), optical modulator and superconducting gate MODFET were shown. Finally because the work done under this URI hinged around our capabiltity to generate, manipulate, and amplify optical pulses, it was necessary to perfect and develop new laser techniques. A good example has been the demonstration and development of chirped pulse amplification .

Also, this URI fulfilled its commitment to education. Between Cornell University and the University of Rochester, nine Ph.D students obtained their degrees under the URI. These students have now a combined expertise in high-speed electronics and optics and they have been sought after by leading laboratories and universities.

In conclusion by fostering quality research and education the program supported by the URI grant brought closer modern photonics and electronics, two fields critical to the nation's future.

Accomplishments of the URI Ultrafast Optical Electronics Center

I. Fundamentals on Electron Transport

A. Transport in Bulk - K. Meyer, M. Pessot, and G. Mourou (Rochester) D. Shire, G. Wicks (Cornell)

Electron-optic sampling of photoconductive transients on a subpicosecond time scale has been used to study hot-carrier transport in GaAs. The results are interpreted as direct time-domain observations of nonequilibrium transport on a subpicosecond time scale and they clearly show both an overshoot and bias-dependent delay at high excitation energy which are consistent with published Monte Carlo predictions.

B. Transport in Layered Structures

1. Resonant tunneling - J.F. Whitaker, G. Mourou (Rochester)

Picosecond bistable operation has been experimentally observed for the first time in a double-barrier resonant tunneling diode. A rise time of 2 ps was measured using the electro-optic sampling technique; this is the fastest switching event yet observed for an electronic device. This time domain measurement adds necessary information to the understanding of the transport mechanisms in the resonant tunneling diode and is consistent with switching time limitations computed for the device. It also demonstrates that appropriately designed double-barrier quantum well diodes have a response time comparable to that of the fastest all-optical logic elements, and that they may be very useful in high-speed logic applications.

2. Tunneling escape time - T.B. Norris, G. Mourou, R.S. Knox (Rochester), X.J. Song, W.J. Schaff, L.F. Eastman, G. Wicks (Cornell)

We have performed time-resolved photoluminescence on $GaAs/Al_xGa_{1-x}$. As single quantum well structures with an electric field applied perpendicular to the well plane. The quantum wells are coupled to the GaAs continuum through a thin barrier; the escape time of the electrons in the well was measured by time-resolved photoluminescence. The dependence of the decay time on applied bias was found to agree very well with a simple semiclassical model.

3. Transport in Asymmetric Coupled Quantum Well - T.B. Norris, G. Mourou, R.S. Knox (Rochester) X.J. Song, L.F. Eastman (Cornell)

We have performed continous and time-resolved photoluminescence experiments on novel double-quantum-well structures in Schottky diodes. We have directly observed the buildup of a charge-transfer (CT) state in which the electron and holes are in separate wells because of the fact that they tunnel in opposite directions. We have studied the effect of an electric field on the CT state formation, and have observed a strong, linear Stark shift of the CT luminescence.

C. Electron-Phonon Relaxation in Metals - H.E. Elsayed-Ali, T.B. Norris, M.Pessot, G. Mourou (Rochester)

Amplified 150-300-fs laser pulses have been applied to monitor the thermal modulation of the transmissivity of thin copper films. Nonequilibrium electron and lattice temperatures have been observed. The process of electron-phonon energy transfer was time resolved and was measured to be 1-4 ps, increasing with the laser fluence.

D. Transport in High-Tc Superconductors - D. Dykaar, J. Chwalek, J.F. Whitaker, T. Hsiang, G. Mourou (Rochester)

Picosecond pulse propagation on transmission lines patterned from $YBa_2Cu_3O_{7-x}$ films has been performed. Distortion-free propagation of high current density transients is demonstrated. The high-frequency properties were analyzed by careful study of the relative phase delays of the electrical transients as the temperature of the sample was varied from 1.8 K to T_c. Simulations using Mattis-Bardeen complex conductivities showed good agreement with the measured results. High-frequency critical current densities in excess of 10^5 A/cm^2 were measured.

II. Ultrafast Techniques

A. Electrooptic Characterization of Devices and Materials - D.R. Dykaar, J. Whitaker, J. Nees, G. Mourou, T. Hsiang, J. Chwalek, M. Frankel, T. Jackson (Rochester), L.F. Eastman, P. Tasker (Cornell)

1. Normal temperature

The electro-optic effect in conjunction with short optical pulses makes possible noninvasive wafer-level testing of integrated circuits. By using this particular technology, testing can be performed over a terahertz bandwidth and with micrometer resolution. Applications to digital integrated circuits and monolithic millimeter-wave integrated circuits (MMIC) have been demonstrated. An external, non-contact electro-optic measurement system, designed to operate at the wafer level with conventional wafer probing equipment and without any special circuit preparation, has been developed. Measurements have demonstrated the system's ability to probe continuous and pulsed signals on microwave integrated circuits on arbitrary substrates with excellent spatial resolution. Experimental measurements on a variety of digital and analog circuits, including a GaAs selectively-doped heterostructure transistor prescaler, an NMOS silicon multiplexer, and a GaAs power amplifier MMIC have been performed.

2. Cryogenic temperature

We have developed a fully cryogenic electro-optic sampler by integrating and immersing in superfluid helium both the photoconductive switch and the birefringent lithium tantalate sensor. The ultimate temporal response of the system as determined by measuring the transient onset of photoconductivity in a GaAs switch was less than 400 fs. The system was arranged into a coplanar transmission line geometry and used to probe the switching of a 30 x 30 μm^2 Josephson tunnel junction. Both time-dependent waveforms of the transmitted signal and current-voltage characteristics of the junction switched by a picosecond input pulse were measured. The results were compared to transient simulations based on the resistively and capacitively shunted junction model, and showed that: the initial junction response was limited only by the time integral of the input pulse, the

switched voltage was proportional to the total charge delivered by the pulse, and there was no turn-on delay time. This represents the first, *in situ* measurement of the response of an unbiased Josephson tunnel junction to a stepped, picosecond pulse.

3. Ultrahigh frequency electro-optic time-domain reflectrometry
We studied a new approach to time-domain reflectmetry utilizing picosecond electro-optic sampling and counter-propagating electrical pulses on a coplanar transmission line. This method enables direct acquisition of the incident and reflected waveforms at the interface between a device and transmission line without requiring temporal separation between the waveforms or deconvolution of the effect of the transmission line on the waveforms.

4. Short electrical pulse generation - J. Whitaker, M. Frankel, S. Gupta, G. Mourou (Rochester)
We have developed a technique for transforming electrical step-like excitations into picosecond electrical pulses by using discontinuities embedded in a coplanar transmission line structure. We have experimentally demonstrated the fomation of 3 ps pulses from photoconductively generated steps. Equations for the pulse amplitude/duration trade-off based on a lumped element approach are given and shown to be in agreement with the calculations of the element values.

B. Short Electrical Pulse Propagation on Transmission Line Studies - J. Whitaker, D. Dykaar, T. Hsiang, G. Mourou (Rochester)

Using a cryogenic electro-optic sampling technique, we have studied the transient propagation characteristics of superconducting and normal indium lines in the picosecond regime. Transient dispersion effects, including increased rise time and increased pulse width, the introduction of ringing on the waveform, and a novel "pulse sharpening" were observed. A model that takes into consideration the effects of modal dispersion and superconducting complex conductivity was established, and an algorithm was developed that accurately describes all of the experimental findings.

C. Picosecond Reflection High-Energy Electron Diffraction (RHEED) - H.Elsayed-Ali, G. Mourou, S. Williamson, R.S. Knox, Hsiu-Chen (Rochester)

Reflection high-energy electron diffraction with picosecond time resolution has been demonstrated. The surface diffraction patterns are obtained using a laser driven picosecond electron gun. Due to the synchronization of the photogenerated electron pulses with the laser source, such a technique provides a picosecond time-resolved surface structural probe sensitive to the first few monolayers.

III. Ultrafast Devices

A. Picosecond Photoconductive Detector - S. Gupta, M. Frankel, D. Dykaar, G. Mourou, and T. Hsiang (Rochester)

A novel material deposited by molecular beam epitaxy at low substrate temperatures using Ga and As_4 beam fluxes has been used as the active layer for a high-speed photoconductive optoelectronic switch. The high-speed photoconductive performance of the material was assessed by fabricating two devices: an Auston switch and a photoconductive-gap switch with a coplanar transmission line. In a coplanar transmission line configuration, the speed of response is 0.5 ps (full width at half maximum) and the response is 10 to 100 times greater than that of conventional photoconductive switches. Since the material is compatible with GaAs discrete device and integrated circuit technologies, this photoconductive switch may find extensive applications for high-speed device and circuit testing.

B. Greater than 100 GHz Traveling Wave Modulator - J. Nees, S. Williamson, G. Mourou (Rochester)

A GaAs traveling wave modulator with a bandwidth greater than 100 GHz has been demonstrated. The dramatic bandwidth enhancement is due to the elimination of the velocity mismatch by the addition of a GaAs superstrate in contact with the optical waveguide.

IV. Laser Technology

A. Femtosecond Pulse Amplfication - P. Bado, S. Coe, J. Squier, D. Strickland, G. Mourou, M. Pessot (Rochester)

A new dye laser and C.W. pumped regenerative amplifier system capable of generating white-light continuum at a repetition rate higher than 1 KHz has been demonstrated. Generation of ultrahigh peak power pulses. Single picosecond pulses have been amplified to the terawatt level by a table-top size Nd: glass amplifier by using the technique of chirped pulse amplification (CPA). The divergence of the beam is twice the diffraction limit, making the brightness of this source equal to $\sim 2 \times 10^{18}$ W/(cm • sr), which is the highest brightness ever reported. The technique of chirped pulse amplification allows the efficient energy extraction from extremely compact amplifier systems. Amplification of chirped pulses over nine orders of magnitude, i.e., from nanojoule to the joule level, has been demonstrated. By using a large-scale Nd: glass amplifier system it should be possible to extend the technique of CPA to the amplifcation of 1 ps pulse to the kilojoule level leading to petawatt power pulses. These pulses, once focused, could produce intensity in the range of 10^{23} W/cm^2, five orders of magnitude over the present state of the art.

URI Ultrafast Optical Electronics Center, Scientific and Technological Program

I. Fundamentals on Electron Transport

A. Transport in Bulk: Velocity overshoot - K. Meyer, M. Pessot, and G. Mourou (Rochester) D. Shire, G. Wicks (Cornell).

Monte Carlo techniques was used to study the transient transport of carriers which were photogenerated by a short optical pulse into a spatially uniform field.[1,2-5] These studies clearly demonstrate that transport transients can be generated by photoexcitation into an applied field. They show an important wavelength threshold associated with electrons photogenerated out of the heavy hole band into Γ-valley conduction states that lie above the threshold for Γ-*L* transfer.[3-5] Such electrons tend to scatter rapidly into the *L* valley and if the field is larger than several kV/cm there is a selection process in which electrons generated into negative velocity states are less likely to scatter to the Γ than those with positive velocities. In this wavelength range the minimum field required for the creation of a velocity overshoot increases, the magnitude of the overshoot decreases,[4,5] and a field dependence in the apparent starting point of the initial velocity appears.[8,9]
For lower fields no overshoot is expected but there is still a prolonged rise in velocity as carriers which initially scattered to the *L* valley return to the Γ valley.[7-10]

All measurements were performed using nominally undoped ($n = 5 \times 10^{15}$ cm^{-3}) high-mobility GaAs grown via molecular beam epitaxy (MBE) at Cornell University or metalorganic chemical vapor deposition (MOCVD) at SPIRE Corporation. Two microns of undoped material was grown on semi-insulating substrates, followed by a 500 Å layer of highly doped ($n = 2\times10^{18}$ cm^{-3}) GaAs. Various test and transmission line structures were patterned using lift-off photolithography. The NiAuGe contacts were furnace annealed in a nitrogen atmosphere, and in conjunction with the doped cap layer formed highly reproducible ohmic contacts, indicated by a quasi-linear dc current-voltage (*I-V*) characteristic to fields as high as 10kV/cm. A calibrated GaAs etch was used to remove the doped cap layer in the photoconductive gaps and between the transmission lines.

Measurement of the transient voltage waveforms generated by the GaAs photoconductive switch was accomplished using reflection-mode electro-optic sampling.[6] In this configuration, illustrated in Fig. 1, a thin plate of $LiTaO_3$ with high-reflectivity dielectric coating on one surface is placed on top of the GaAs sample with the coating in contact with the GaAs. A small window (not shown in the figure) was etched in the coating to allow for passage of the excitation beam to the photoconductive switch. The probe beam was focused between the transmission lines a short distance from the gap. When there is a voltage on the transmission line, fringing electric fields from the substrate extend into the electro-optic superstrate and are a rotation of the polarization of the probe beam.

Results obtained with 620 nm photoexcitation (electron energy = 520meV) are shown in Fig. 2, plotted as the measured transient voltage normalized to the gap voltage. The excitation density was approximately 5×10^{17} cm^{-3}. The transient voltages were only on the order of 0.01% of the applied voltage, indicating that the perturbation of the electric field was small. Two features are clearly apparent in the data: a significant photocurrent overshoot that occurred at high bias but not at moderate or low bias, and a much faster rise

time of the transient for higher bias. Both of these features are consistent with Monte Carlo predictions, as will be discussed below.

Theory predicts that photoexcitation closer to the conduction-band edge will result in a larger velocity overshoot, because the electrons will spend more time in the Γ valley, where their mobilities are higher, before they scatter into the Γ valley. For this reason it was desirable to repeat the experiment at a longer excitation wavelength. Photocurrent transients obtained with 760 nm excitation (electron energy = 190 meV) are shown in Fig. 3. Once again, a photocurrent overshoot was observed at high applied field but not at low field. The observed degree of overshoot was not as large as anticipated, probably because the temporal resolution in this case (determined primarily by the laser pulsewidth) was insufficient to fully resolve the rise of the transient.

In summary, the experiment described here provides a transient time-domain measurement with excellent temporal resolution. The data are consistent with an interpretation that calls for a photocurrent overshoot. The features of this overshoot are consistent with the hypothesis that they are largely the result of transport transients, i.e., electron velocity overshoot.

B. Transport in Layered Structures

1. Resonant Tunneling - J.F. Whitaker, G. Mourou (Rochester)

We have performed the measurement of a double=barrier resonant tunneling diode (RTD) in its bistable or switching mode with sufficient temporal resolution to resolve the switching time. We have measured this switching time to be less than 2 ps. This time compares favorably with the theoretical considerations of Liu and Coon[7] for the switching time of a heterojunction double-barrier diode circuit. These time domain measurements provide some insight concerning the mechanisms of electron transport through double-barrier heterostructures, processes that are far from being completely understood.

The RTD used in these measurements was grown by molecular beam epitaxy to have two barriers of 1.5-nm-thick AlAs separated by a GaAs well 4.5 nm thick. The outer regions of GaAs contained Si doping to an electron density 2 $\times 10^{17}$ cm^{-3}. This resulted in a peak current density of about 4×10^4 A/cm^2. For the 4-μm-diam RTD tested here, the capacitance when biased near the current peak was calculated to be 20 fF, and a series resistance was 15Ω. More details of the material growth and fabrication can be found in Ref. 8.

The device was tested using an instrument with the subpicosecond resolution necessary to measure such brief events, the electro-optic sampling system.[9] A schematic diagram of the circuit used to test the time response of the RTD is shown in Fig. 4. Coplanar electrodes of gold acting as a transmission line were deposited on both a GaAs switch and a lithium tantalate ($LiTaO_3$) sampling crystal, and the bias to the RTD was applied through a large inductor, and the bias from a GaAs photoconductive switch was considered as the input to the network.

The method used to determine the switching time of the device will now be presented. The region between the two load lines labeled "1" in each frame of Fig. 5(a) represents the shift in load line resulting from closing the switch with the optical pulse, when starting from different dc bias conditions. The region labeled "2," shown in the top frame only, indicates the shift in load line along a relatively linear portion of the *I-V* curve.

The resulting waveform from region 2 as the output of the diode was used as a reference so that a comparison could be made to each of the other waveforms from region 1 and the switching response more easily resolved. This waveform 2 is depicted in each of the frames of Fig. 5(b). Displayed as a dashed line is the waveform from each region 1 in Fig. 5(a) and, below the waveforms, the temporal variation of the difference of the two waveforms. The waveforms in Fig. 5(b) are exaggerated to schematically show the effects of switching. the experimental result of subtracting the two waveforms from regions 1 and 2 is presented in Fig. 5(c). In the first frame, the cancellation is nearly complete. The discrepancies observed are due to noise and to small deviations in the regions of the *I-V* curve traversed. The switching process can be observed in the second and third frames of Fig. 5(b) and 5(c). In the second frame, curve 1, the dashed line, follows curve 2 only from points *A* to *B*, where it coincides with the rising portion of the *I-V* curve. When the load line exceeds the current peak of the *I-V* curve, the diode switches to point *C* and a rapid drop in the current is observed. In the second frame, as the input decreases, the optical switch current also decreases so that the load line drops below point *E*, and the operating point returns to *F* and relaxes to *A*, where waveforms 1 and 2 are again nearly identical. This is indicated in the different waveform (1-2) of Fig. 5(b) and can also be seen in the experimental difference waveform in Fig. 5(c).

The third frame of Fig. 5 displays the same switching action, but with the device attaining a latched state. The operation from points *C* to *D* to *E* is along a path of the *I-V* curve that would approximately cancel with that from region 2, leading to a long plateau on the difference waveform and a device that has been switched into the lower current state. This was distinctly observed in frame 3 of Fig. 5(c). Since the peak of the *I-V* curve was reached by the load line earlier than in the frame above, the switching took place at an earlier time, as evidenced by the position of the waveforms relative to the thin vertical line of Fig. 5(c) that represents a constant time reference. In frame 2, the onset of the switching began at the marker, while in frame 3 the switching event was already about halfway completed. The rise time of the switching event, as measured from the third frame of Fig. 5(c), was discovered to be 1.9 ps in duration between the 10% and 90% points. During the relatively long time between optical pulses, the bias point returns to point A. This is possible because the impedance determining the low-frequency load line is much smaller than the high-frequency impedance. In frame 4 of this figure, the dc bias point is extended above the area of negative differential resistance, where region 1 traverses virtually the same slope as region 2, and cancellation is again expected and found.

As mentioned earlier, the switching time should depend on the time to charge the device capacitance between the voltages corresponding to point A and C in figure 5(a).[7,10]

$$t_s \approx C(V_C - V_B)/(I_p - I_v), \tag{1}$$

where I_p and I_v are the peak and valley currents in the negative differential distance region. As measured experimentally, $V_C - V_B$ - 0.44 V and $I_p - I_v = 3$ mA. Charge storage occurs predominantly outside the double-barrier region, and so to compute the capacitance, we must know the distance between the conductive regions on each side of the quantum well. The GaAs well width was 4.5 nm, while the AlAs barriers were 1.5 nm thick, and the depletion width into the doped collector region was approximately 70 nm. Using a relative permittivity for GaAs of 13.1, the capacitance was found to be about 20 fF, and the rise

time for switching was calculated to be 2.9 ps. Bearing in mind that Eq. (1) is only approximately valid and that the instrumental contribution was not measured, this is in reasonable agreement with the measured value of 1.9 ps.

The tunneling current in a RTD can be a result of a resonant, coherent tunneling current, as in the optical analog of a Fabry-Perot resonator, and/or a sequential, incoherent tunneling process stemming from elastic and inelastic collisions. Originally, the idea of electrons scattering and sequentially tunneling was used by Luryi[11] to explain the discrepancy between the measured and expected current of the device. It was pointed out by Weil and Vinter[12] and Jonson and Grincwajg[13] that, in most cases, the tunneling current is proportional only to the resonant level linewidth Γ_r and insensitive to the scattering energy width Γ_i. The device response time, however, in inversely proportional to the total energy width of the system, $\Gamma_t = \Gamma_r + \Gamma_i$. The measured switching time can be looked at as an upper limit of the response time of the structure, since the measurement circuit could only increase the time of response. In our experiments, the device tested had a geometry such that Γ_r was about 2 meV. The resulting device response from resonant tunneling alone ($t \approx 2\hbar\Gamma_t$) could therefore be of the order of a single picosecond. Thus we can make no statement about the importance of sequential tunneling from this measurement. However, if a RTD with a much smaller Γ_i were to show a switching time of a picosecond or so, then we could conclude that sequential tunneling was the dominant transport mechanism, since this process would give us the very fast response commensurate with the collisionally broadened Γ_i.

In conclusion, we have used the electro-optic sampling technique to measure the fastest switching event yet for an electronic device. The switching speed of the RTD is also comparable to the one observed in the fastest optical bistable devices. The similarity in the observed performance of the electronic and optical bistable devices is not surprising considering the fact that the switching time is limited by the round-trip time in the Fabry-Perot resonant cavity. That is, the nanometer dimensions and slow electron velocity of a RTD provide comparable round-trip times to those obtainable with the submicron dimensions but higher photon velocities of multiple quantum well optical devices. This illustrates just how similar electrical and optical resonators are, and how the response of electronic devices is catching up to the supposedly faster optical devices.

2. Tunneling Escape Time of Electrons from a Quantum Well Versus Field - T.B. Norris, G. Mourou, R.S. Knox (Rochester), X.J. Song, W.J. Schaff, L.F. Eastman, G. Wicks (Cornell).

There has been much theoretical work regarding the time dependence of tunneling; however, very little time-domain experimental work has been done. Tsuchiya *et al* [11] have studied the decay of an electron localized between two thin barriers in a single GaAs/AlAs quantum well (QW) structure using a technique of picosecond time-resolved photoluminescence (PL). They found that for sufficiently thin barriers, the PL decay time matched the tunneling time predicted from the calculated width of the resonant state. Of course, in the double-barrier structures commonly studied, a strong electric field is applied perpendicular to the QW plane. In the semiclassical model, the tunneling rate $1/\tau_T$ can be expressed as the product vT of the frequency v of the electron collisions with the barrier and the tunneling probability T through the barrier. The tunneling coefficient T is expected to decrease strongly with an applied field, and consequently an increase in the tunneling

rate should be observed. We have investigated this field dependence using time-resolved PL.

The PL decay rate can be expressed as

$$1/T = 1/\tau_T + 1/\tau_R, \tag{2}$$

where τ_R is the electron-hole recombination (radiative and nonradiative) time, which is of the order of a few hundred picoseconds subject to trap levels and the injected carrier density.[12-14] However, the escape time τ_T is quite independent of those effects and would be equivalent to the measured PL decay time if it were much faster than τ_R. The QW structure is designed so that τ_T lies between the streak camera limit (20 ps) and the recombination time (subnanosecond).

The structure of the samples under study is shown in Fig. 6. A single 30 Å GaAs QW is bounded on one side by a thick (0.2 μm) $Al_xGa_{1-x}As$ barrier, and on the other side by a thin $Al_xGa_{1-x}As$ barrier and a 0.1-μm-thick GaAs region. This undoped structure was clad between 0.1 μm p^+ cap layer and a 1 μm n^+ buffer layer grown on top of the semi-insulating (SI) substrate. Tunneling is only possible through the thin barrier beneath the QW.

The samples were held in a cryostate at a temperature of about 6 K. The PL was imaged through a 0.32 m grating monochromator (300 l/mm grating) onto the entrance slit of a Hamamatsu synchroscan streak camera with a two-dimensional intensified detector array. In this way we could obtain the time-resolved PL spectrum with a time resolution of approximately 20 ps; a typical data run is shown in Fig. 7.

Our experimental results may be understood with a straightforward semiclassical model. In general, the tunneling time of bound electron through a barrier may be approximately expressed as

$$\tau_T = c \exp\left(\frac{2}{\hbar}\int_0^b \sqrt{2m\,(V - E - Fz)\,dz}\right), \tag{3}$$

where b is the barrier thickness, F is the applied field, and c is a constant.[15]

We have calculated the integral for our sample parameters; the results are the solid lines in Fig. 7. We have made an approximation that c and E do not change appreciably with the electric fields considered here. The proportionality constant was obtained by calculating the transmission coefficient T for a barrier under flatband conditions, and using the relation $\tau_T = (\nu T)^{-1}$ for the tunneling time at zero bias. The expression for the transmission coefficient under flatband conditions is

$$T = \frac{4r(V - E)E}{[(r - 1)E + V]^2 \sinh^2\left[(b/\hbar)\sqrt{2m_B(V - E)}\right] + 4r(V - E)E}, \tag{4}$$

where $r = m_B/m_W$, and $m_B(m_W)$ is the effective mass in the barrier (well). Also, the oscillation frequency of the electron in the well is given by

$$\nu = (1/d)\sqrt{E/2m_W}\,. \tag{5}$$

For our structure, v is $1.3\times10^{14}s^{-1}$. We have assumed that 65% of the total band offset is in the conduction band. The results were $t_T(0)$ = 809, 277, and 17 ps for the 121, 111, and 85 Å barrier samples, respectively.

The curves plotted in Figs. 7(a) and 7(b) use the calculated values of the zero-bias tunneling time; hence there are no free parameters determining these curves. For the theoretical curve in Fig. 7(c), we have assumed the zero-bias tunneling time of 65 ps rather than the calculated value of 16 ps. For the field dependence on the bias voltage, we have simply used for these curves $F = V/d$, where V is the applied voltage and d is the depletion width determined by C-V measurements. We find that the field obtained at -2V bias was 5×10^4V/cm. It should be noted that a quantitative fit to the data is difficult because small uncertainties in MBE growth rates and band offset values will result in large differences in the calculated tunneling rate. Furthermore, a precise determination of the electric field at the location of the quantum well is very difficult. It should also be noted that we have not considered the effect of the exciton binding on the tunneling rate[16]; this may be important for structures with narrow barriers. Nevertheless, it is apparent that the simple theoretical expression (2) properly displays the field dependence of the tunneling rate.

We finally note that our time-resolved PL spectrum data allow us to also measure the PL Stark shift with applied field. We have studied one structure which showed no measurable tunneling (b = 85Å and x = 50%), and the usual red shift of the PL with applied field was observed.[17] However, in all tunneling samples discussed here, a small *blue* shift was observed (peaking at about 3 meV for fields in the range $2\text{-}4\times10^4$ V/cm). To our knowledge, this is the first observation of a blue shift in the PL from a quantum well with an electric field; further study is necessary to determine the physical origin of this shift.

In conclusion, we have observed an increase in the tunneling rate of bound electrons through a thin barrier in the presence of a perpendicular electric field. The behavior of the tunneling rate versus electric field is in good agreement with the predictions of a semiclassical model. This measurement is important for the complete understanding of the dynamics of tunneling in double-barrier heterostructures.

3. Transport in Asymmetric Coupled Quantum Well - T.B. Norris, G. Mourou, R.S. Knox (Rochester) X.J. Song, L.F. Eastman (Cornell)

We have observed the direct observation of the buildup of a "charge-transfer" (CT) state via electron and hole tunneling in opposite directions in GaAs/$Al_xGa_{1-x}As$ double QW structures.

The double-QW structures used in this study are of a novel design, where the two QW's are of different widths, but the Al composition of the wider QW is adjusted so that under flat-band conditions the electron energy levels of the two wells are very close to resonance, and the hole energies are sufficiently different so that the PL energies of the two wells separated.[18,19] A 58-Å $Al_{0.15}Ga_{0.85}As$ QW (QWI) is coupled to a 26-Å GaAs QW (QW2) through an $Al_{0.45}Ga_{0.55}As$ barrier. Two samples were grown for this study: Sample *A* has a thin (43-Å) barrier so the electron states are somewhat delocalized over the two wells, and sample *B* has a thick (86-Å) barrier so the electron states are strongly localized in each QW. Twenty-five periods of the double-QW structure were grown on an n^+-type GaAs substrate and n^+-type GaAs buffer layer. A semitransparent Al Schottky

contact was evaporated on the top surface so that the effect of an electric field applied along the growth direction could be studied. The calculated band diagram and electron and hole states for sample *A* are shown in Fig. 8 for both flat-band and reverse-bias conditions.

The samples were held in a cryostat at a temperature of 6 K. Photoexcitation was provided by picosecond pulses from a synchronously pumped dye (Pyridine 1) laser. We estimate that each laser pulse injected a carrier density of approximately 10^{11} cm^{-2} in each well.

CW PL spectra are shown for both samples in Fig. 9. For sample B the ω_1 and ω_2 transitions are about the same magnitude, but for sample *A*, the ω_1 intensity is much smaller than for ω_2, indicating stronger tunneling processes for this sample, as will be discussed below.

Time-resolved spectra for sample *B* (thick barrier) are shown in Fig. 10 for 0 and -8 V bias. The spectra show the scattered pump light (defining the time origin) and two PL lines corresponding to recombination within each of the two wells. The high-energy PL line corresponds to the QW1 transition, and the lower-energy line to QW2. The PL rise and decay times change very little with applied bias, and the Stark shift of the PL peaks is observed to be a few meV to the red as expected.[21-22] In the CW PL spectra shown in Fig. 11, however, we observe a third PL peak which shifts strongly and approximately linearly towards the red with applied bias. In the narrow barrier sample (*A*) this peak appears even more clearly in the CW spectra and presents a stronger Stark shift. The origin of this peak can be elucidated by examining the time-resolved PL spectra for the thin barrier sample; the line comes from radiative recombination between electrons in QW1 and holes in QW2, which we refer to as the charge-transfer (CT) state.

A selection of the time-resolved PL spectra versus applied bias voltage is shown in Fig. 12 for sample *A*. At low bias one sees the scattered pump light and two PL lines corresponding to the ω_1 and $\omega_2 + \omega_{CT}$ transitions. It should be noted that at resonance the PL of QW2 and the CT state have the same energy. As the electric field is increased, the ω_2 and ω_{CT} lines separate and ω_{CT} is strongly Stark shifted to lower energy. The Stark shift of this long-lived PL component is approximately linear with applied bias. The strong red shift and long decay time indicated that this PL is, in fact, the result of recombination of electrons and holes in the CT state. The CT state is built up by electrons tunneling from QW2 to QW1 and holes tunneling from QW1 to QW2. The long lifetime is the result of the small overlap of the electron and hole wave functions, but the Ct luminescence is nevertheless observable due to the nearly complete charge separation that takes place. This explains why the CT luminescence is observable in the CW PL spectra but not in the time-resolved spectra for sample *B*. In this case the charge separation is no so strong due to the much slower electron and hole tunneling rates between the wells, so although the long-lived radiative recombination is observed as a line in the CS P1 spectrum, the instantaneous intensity is low and therefore extremely weak on the time-resolved spectrum.

In summary, we have performed time-resolved and CW PL spectroscopy on a novel double-QW structure, and have directly observed luminescence from a charge-transfer state, where the charge separation occurs by electron and hole tunneling in opposite directions induced by the electric field.

C. Electron-phonon in Metal

We report results obtained using amplified 150-300-fs laser pulses to resolve in time the electron-phonon relaxation by monitoring of the laser-heating-induced modulation of the transmissivity of thin copper films. The time resolution was sufficient to resolve electron-phonon coupling in copper. In addition, the laser energy (up to 0.3 μJ per pulse) was sufficient to produce up to a few thousand degrees electron and lattice temperatures.

The experimental setups in shown in Fig. 12 observed time-resolved transmissivity of a 200 ± 50-Å copper film at $\lambda \simeq 620$ nm during laser heating (~ 300 fs FWHM) for a variable pump-probe fluence is shown in Fig. 14. The initial response of the transmissivity appears to be integration of the heating pulse. The rise time of the initial transient was shorter for ~ 150-fs (FWHM) heating pulses, consistent with the above-mentioned observation. The decay of the fast transient was found to be 1-4 ps, increasing with the heating-pulse fluence. This effect is due to larger differences between electron and lattice temperatures for higher fluences; thus, more electron-phonon collisions are required for thermalization. A much slower decay of the lattice temperature (mainly due to diffusion) was observed following the initial fast transient. Possible effects due to modulation of the optical properties of the substrate during laser heating were checked by the performance of the experiment with an uncoated glass slide. For conditions used in Fig. 14 and for our resolution limit, no modulation of the transmissivity of the substrate was observed.

For conditions used in the present work where the laser pulse width was shorter than the electron-phonon relaxation time, the time evolution of the electron and lattice temperatures can be described by two coupled nonlinear differential equations.[23]

$$C_e(T_e)\frac{\partial T_e}{\partial t} = k\Delta^2 T_e - G(T_e - T_l) + P_0(r,t), \tag{6}$$

and

$$C_l \partial T_l/\partial t = G(T_e = T_l). \tag{7}$$

The electronic heat capacity, $C_e(T_e)$, is proportional to the electron temperature [$C_e(T_e) = 9.6.6T_e$ J/m^3·K].[24] The first term on the right-hand side of Eq. (1) represents thermal-conductivity losses. As a result of the thin-film geometry used in our work, thermal conductivity is thought to have a negligible contribution at the time scales of interest (few picoseconds after the laser-heating pulse) and can be ignored. The second term in Eq. (1) represents electron-phonon coupling. The coefficient of heat transfer between the electrons and the lattice,[25] G, is assumed to be constant for our experimental conditions and is obtained by a comparison of the experimental data with the model. The third term in Eq. (1) represents the laser-heating source. Measurements showed that at $\lambda = 620$ nm, 5% of the normally incident radiation is absorbed in the copper film at room temperature. Small deviations in this value due to laser heating are ignored in the present model. In the present calculations, the lattice heat capacity, C_l, had a value of 3.5×10^6 J/m^3·K.[24]

Equations (1) and (2) were solved numerically. Time evolution of the electron and the lattice temperatures for different values of electron-phonon coupling constant, G, and for conditions used in Figs. 14(b) and 14(e) are shown in Figs. 15(a) and 15(b). The laser-heating pulse was assumed to be Gaussian with a FWHM = 0.3 ps and peaking at 1 ps. Clearly, the electron-phonon relaxation time is strongly dependent on the value assigned to G and increases with a decrease in the electron-phonon coupling constant. In

addition, the electron-phonon relaxation time was found to increase with the applied heating-laser fluence which is consistent with the experimentally observed results. Since the electron-phonon relaxation times considered in the analysis are larger than the laser-heating pulse width, the peak electron temperature had only a small dependence on the value of the electron-phonon coupling constant. Although the equilibrium electron and lattice temperatures predicted by the model were directly proportional to the heating-laser fluence, the peak electron temperature had nearly a square-root dependence on the laser fluence. Indeed, deviation from this square-root dependence is due to the fact that some electron-phonon energy transfer does take place during the laser-heating pulse. Thus, this deviation from square-root dependence is enhanced for larger values of G.

Comparison of the time-resolved thermomodulation-transmissivity measurements of the time required for the electrons and the lattice to reach equilibrium with that predicted by the model indicates that G has a value of $\sim 1\times10^{17}$ W/m^3·K. For a pulse energy of 65 nJ (peak fluence of $\simeq 3.8\times10^{10}$ W/cm^2), the model predicts a peak electron temperature of 2200 K and an equilibrium electron-phonon temperature (ignoring conduction losses) of 385 K. Although this simple model seems to be consistent with the experimental observations, more accurate modeling can include the modulation of the deposited laser energy due to the thermal modulation of the optical properties of the film, in addition to accounting for the small dependence of G and C_l on temperature.

In conclusion, we have used the thermal modulation of the transmissivity of thin copper films to measure the electron-phonon relaxation time in copper as a function of pump-laser fluence at λ = 620 nm and as a function of probe photon energy for λ = 560 - 640 nm. We have demonstrated nonequilibrium heating with up to a few thousand degrees difference between electron and lattice temperatures. Additional studies are needed to actually relate the modulation of the optical properties of metals with electron and lattice temperatures.

D. Transport in High-Tc Superconductors - D.Dykaar, J. Chwalek, J.F. Whitaker, T. Hsiang, G. Mourou (Rochester)

Studies of the high-frequency properties of YBCO materials, based on response of the superconductors to microwave frequency electromagnetic perturbations, are of special interest, because they can give insight into the exact nature of the energy gap, quasiparticle excitation, and the pairing mechanism. From the applications point of view, simple extrapolation of the Mattis-Bardeen theory predicts, for example, distortion-free propagation of electrical pulses having bandwidths of tens of terahertz. The first published experiments[27,28] were performed on bulk, ceramic samples and showed reasonable agreement with the BCS theory in the very dirty limit.[27] However, the results were very strongly influenced by the granular, not fully controlled nature of the tested samples.[28] Workers at IBM recently reported results with aluminum lines and a YBCO ground plane,[29] showing no absorption for the pulses propagating on the normal aluminum lines.

For an ordinary Bardeen-Cooper-Schrieffer (BCS) type superconductor, the energy-gap frequency at zero temperature, $f_G(0)$ is related to the transition temperature T_c by $f_G(0) = 3.52\ K_B T_c/h$, where K_B is Boltzmann's constant, h is Planck's constant, and 3.52 is a constant which varies from material to material.

One can easily see that for BCS type behavior the above equation gives a value of the energy-gap frequency in the *tens of terahertz* for transition temperatures of ≈ 90 K. This transition temperature is now routinely achieved in the new $YBa_2Cu_3O_{7-x}$ (YBCO) ceramic[26] although the exact nature of the coupling mechanism for the YBCO material is still controversial.

We report our preliminary studies of picosecond electrical transients propagated on thin-film, coplanar transmission lines made out of the YBCO material.

The experimental setup, based on the electro-optic sampling technique, was similar to the one used to study picosecond transient propagation on In coplanar lines,[30] and is shown in Fig. 16. In sample 1, the photoconductive switch was placed on top of the substrate and wire bonds were made down to the transmission lines. The faster response measured in sample 2 was due to the planar configuration of the switch and sample which allowed very short, planar wire bonds from the switch to the input of the transmission line. The sampling was done in a reflection mode which employed two high-reflection dielectric coated $LiTaO_3$ crystals (located at either end of the transmission lines) which served as the sampling points for the input and output transients, respectively. In this particular configuration the wire bonds, together with the contact pads, act as a low-pass filter. Thus, our electrical pulse rise time (as measured at the "input" $LiTaO_3$ crystal) was limited to about 15 ps for the first sample and to about 5 ps for the higher speed geometry used in sample 2.

The measurements of sample 1 were done with the sample immersed in superfluid helium. For a given switch signal, we carefully measured both the input and output transients (here we define input and output as measured at the corresponding "input" and "output" $LiTaO_3$ crystals). This result, shown in Fig. 17, clearly shows that a YBCO transmission line can support distortion-free propagation of picosecond electrical pulses over a substantial propagation distance. We could easily propagate undistorted signals having rf current densities greater than 10^5 A/cm^2, being limited by our ability to produce larger amplitude input signals. In order to measure the temperature-dependent critical current, a current density of 4×10^4 A/cm^2 was maintained as the temperature was increased. When the rise time began to decay, the critical current density had been reached for that value of transition temperature. At this current density the rise time showed no degradation until a temperature of 17-18 K was reached. For comparison, at room temperature the same transmission line was characterized by an input rise time of the order of 150 ps and the output signal was severely distorted and reduced in magnitude by almost 30 times.

In a subsequent experiment (using sample 2) we slowly warmed the sample and measured the output transient as a function of temperature for a *fixed* input pulse. As shown in Fig. 18, there is substantial dispersion in this experiment. The degradation in signal rise time (from 5 to ≈ 19 ps) in propagating through the transmission line structure does not depend on the temperature, which implies that the longer rise times are not due to the YBCO film but to other loss mechanisms such as substrate loss. For current densities of 1×10^4 A/cm^2, degradation of the output waveform did not occur until temperatures > 65 K were reached. These waveforms were then simulated using a previously reported numerical simulation program, which has been used extensively to model propagation on ordinary superconducting transmission lines.[30] By using loss tangent values as high as 0.17, good agreement is achieved between measured and simulated values of the phase

velocity versus temperature. The percent change in phase delay, as calculated relative to the initial delay at a temperature of 1.8 K, is plotted against temperature and is shown in Fig. 19. The percent change was found to be very weakly dependent on the substrate parameters and very strongly dependent on the YBCO superconducting parameters. For the simulation, the average dielectric constant = 12, the energy gap (Δ) is 0.0175 eV, T_c = 78 K, and the normal state resistivity of 3×10^{-3} Ω cm (taken directly from dc current-voltage measurements). While different methods yield $\Delta_{YBCO} = 2.25\ kT_c$ to $6\ kT_c$, the corresponding gap frequency is so much greater than the frequency content of our signal that there is a negligible effect on the results due to a variance in Δ (changing Δ by a factor of 2 produced little effect). Also evident in the figure is a slight underestimation of the delay in the simulations at temperatures near T_c. This is likely due to the fact that in the experiment there are finite current densities and in the simulation it is assumed that the current density is zero. Zero dc resistance was measured at a temperature of 78 K.

In the first sample, the losses due to the substrate were negligible. This can be seen by comparing the input and output waveforms of Fig. 17 with those of Fig. 18. The difference in performance of the two substrates appears to be due to the processing variations that the samples were subjected to. Sample 1 had no defects in appearance while sample 2 was covered by a residue which may have contributed to the high losses measured in the experiment.

The high current densities and low attenuation measured in this study are consistent with a Mattis-Bardeen interpretation using complex conductivities, as these parameters are virtually constant well into the tetrahertz range. Since the BCS energy gap for a 90 K superconductor is ~ 20 THz, there should be negligible attenuation in the frequency range used in this work. However, significant changes in the phase velocity as a function of frequency would lead to dispersion at "lower" frequencies (a few THz). In addition, modal dispersion[8] becomes an increasingly important distortion mechanism as bandwidth and/or propagation length increases.

In conclusion, we have presented the first measurements of high-frequency propagation in thin-film oxide superconducting transmission lines. We demonstrated the possibility of propagating undistorted signals on such lines at current densities in excess of 10^5 A/cm^2 limited by the photoconductive switch. The results were successfully simulated using Mattis-Bardeen complex conductivities.

II. Ultrafast Techniques

A. Electro-optic Characterization of Devices and Material - D.R. Dykaar, J. Whitaker, J. Nees, G. Mourou, T. Hsiang, J. Chwalek, M. Frankel, T. Jackson (Rochester) L.F. Eastman, P. Tasker (Cornell)

1. Normal Temperature

The characterization of both devices and circuits in the millimeter-wave range and beyond requires instrumentation possessing unprecedented resolution. An external, non-contact, non-destructive, relatively non-invasive[48,49] technique can be used to make rapid measurements of electrical quantities, including the S-parameters of a circuit or device. This external electro-optic sampling technique closely approaches the ideal probe for integrated circuits: applicability to circuits fabricated on any substrate; high temporal

resolution so that one measurement can cover all frequencies of interest; high spatial resolution for ease of testing small structures; no contact requirements so that probing of internal nodes may be accomplished; low perturbation of signals in the circuit; table-top, room temperature test environment; compatibility with low-temperature testing.

The probing technique indicated employs an extremely small electro-optic crystal as a proximity electric-field sensor, determining electric potential by measuring the strength of the fringing electric field.

The positions of the electro-optic probe beams for two *different* sampling configurations are shown in Fig. 20(a). The transverse crystal, which would be made of lithium tantalate (LT), is used to measure a fringing e-field perpendicular to the probe beam, while the longitudinal crystal, fabricated of deuterated potassium dihydrogen phosphate (KD*P), is used to measure field components that are parallel to the probe beam (perpendicular to the surface of the electrodes). When the latter tip is used, the most accurate measure of the potential of that electrode carrying the broadband waveform is obtained. Figure 20(b) indicates the relative field strength measured over each of the electrodes of a coplanar waveguide using the two electro-optic probes. The longitudinal probe, which may be reflected off of an electrode rather than a high-reflectance coating as shown in Fig. 20(a), is seen in Fig. 20(b) to measure the e-field corresponding to +V only over the extent of the center conductor. The transverse probe tip, however, is used to measure the field normal to the probe beam so that +V is only found over a small range of position directly between the electrodes. The longitudinal tip therefore is able to determine the voltage much more quickly and accurately by sensing the e-field over an arbitrary position of a line, while it is also immune to cross-talk fields from neighboring transmission structures.

The external electro-optic testing technique has been applied to several integrated circuits in order to prove its utility. The first of these to be discussed is a digital circuit, a GaAs selectively-doped heterostructure transistor prescaler. In this case, waveforms on a transmission line with 4-μm features at the output of the input buffer of the circuit were measured. The buffer consisted of two banks of three inverter stages, each generating clock and complementary clock output signals. Each inverter consisted of two transistors, one for switching and one for an active load. Measurements were made at this internal node of the circuit on small lines in order to show that signals could be proved with excellent spatial resolution at points inaccessible to conventional "Cascade-type" proves. Fig. 21 demonstrates the buffer output when a 1.0-GHz continuous signal is input to the circuit, and the dc bias is varied from above the switching threshold of the inverter chain (where V_{th} for each inverter is 0.4 - 0.5V) to below threshold.

A 1.0-GHz clock waveform was also measured on-chip across a 4-μm space between an input clock line and an adjacent power supply line in a high-speed NMOS silicon 12-bit muliplexer. This sine wave, shown in Fig. 22, is an example of a non-contact, electro-optic measurement of a signal in an integrated circuit having a non-electro-optic substrate material. (i.e., not GaAs, as used in ref. 50). The clock signal was approximately 200 mV peak-to-peak, and it was generated by phase-locked microwave driver circuitry and scanned at a 1-kHz rate. In this particular case, 100 scans have been averaged in 400 ms and an excellent signal-to-noise ratio has been obtained.

Measurements were also made on several millimeter-wave, monolithic microwave integrated circuits (MMIC). In this case the signal to be measured was not a synthesized

sinusoidal waveform, but rather it originated at the output of a photoconductive switch excited by another 80-fs laser pulse split off from the optical probe beam. Electrical signals with extremely short rise times can be generated in this fashion[51]. These step impulses were introduced to the first-gate of 0.4μm-gate-length MESFET in Texas Instruments 100-mW, single and double stage power amplifier MMICs. The output electrical signals were then probed above the microstrip transmission lines at the outputs of the amplifier stages. Fig. 23 displays the Fourier transforms of the measured time-domain waveforms for three different drain voltages in the signal stage MMIC. Similar waveforms were obtained at the outputs of the first and second stages of the two-stage amplifier, with the latter exhibiting greater amplitude. Gain over a narrow band centered at 32.5 GHz was observed. In this case an optical rail provided the variable delay between the probe beam and the excitation beam for the photoconductive switch. Each scan of the delay between the probe beam and the excitation beam for the photoconductive switch. Each scan of the delay rail provides data points that are displayed versus time on a signal averages; a scan normally takes seconds to complete.

We have demonstrated that the technique of external electro-optic sampling can be useful for probing microwave signals on integrated circuits fabricated on arbitrary substrates, having various open-boundary electrode configurations with few-micron dimensions. In addition, it has been shown that the electro-optic probe tip can measure voltage values on an integrated circuit chip, even in areas where physical contact made by a test instrument would be inappropriate. Measurements in excess of 100 GHz are easily within the capabilities of the electro-optic sampling technique, as future work will prove.

2. Electro-optic sampling for cryogenic electronics

We report the cryogenic implementation of the electro-optic sampler and its applications to testing superconducting devices and circuits. The design represents a natural extension of the room-temperature system into the low temperature environment. All performance parameters of the room temperature version of the sampler, such as subpicosecond resolution and microvolt sensitivity[52] are either improved or remain unchanged in the cryogenic version. The measured temporal response of less than 400 fs represents the fastest electrical transient ever measured at cryogenic temperatures.

In our first attempt, a simple setup was designed using a coaxial-type geometry with the sampling crystal placed in a cut cable just above the liquid helium level.[53] Using 2-mm (0.085 in.) diameter semirigit coaxial cable and 40 GHz connectors, a system rise time of 16.4 ps was measured. This relatively slow response was a direct result of the long cables (about 1m) required to route the signal from the room-temperature switch into the dewar.

The next step was to integrate the switch and the sampling crystal.[54,55] Several structures were considered. The reflection mode geometry [54] was tried first. In this geometry the sampling crystal is coated with a dielectric reflective coating. The gapless structure allowed the switch to be defined by the laser excitation beam spot rather than by a predefined gap made into the switch. In addition to allowing very short propagation distance, this structure provided flexibility in changing the propagation path length. A sampler made in this geometry, using lead electrodes, had a measured rise time of 1.8 ps at room temperature. However, it became apparent that it was difficult to properly align the laser beams inside the dewar, and so different geometries were explored. (We note that a

similar design has been adopted recently by Gallager et al[56] who took full advantage of the gapless structure).

The final geometry chosen for most of the experiments is a coplanar transmission line. This geometry has also been used at room temperature, with a measured rise time of 460 fs.[55] In this design, the switch and sampling crystal were edge-polished until a mating surface was produced with micron uniformity. These were then glued down onto a microscope slide, and surface polished. The resultant structure was so uniform that metal electrodes could be evaporated continuously across the interface. The sampling test structure was fabricated using photolithographically defined 20 μm indium lines. The measured time resolution of this test structure was 360 fs, as shown in Fig. 24.

Most electrical signals of interest are in the volt or even millivolt range, whereas the halfwave voltage for the modulators (Pockels cell) used is in the kilovolt range. Significant sensitivity enhancement is therefore needed.

The first step is provided by the laser itself. With a repetition rate of 100 MHz, small signals can be quickly integrated by the photodiodes into large ones. Next, a lock-in amplifier is used to move the integrated diode signal into a frequency regime of low electronic noise.

The lock-in amplifies a particular frequency used for modulating either the bias of the photoconductive switch or via an acousto-optic modulator, the excitation pulse train. Our latest version uses a mixing technique in conjunction with the low-frequency, high-sensitivity lock-in amplifier, which allows detection of signals in the 2-4 MHz region. The advantage of this scheme is that the modulation frequency can now be chosen to be above the 1/f region of the CPM noise spectrum (with the 1/f noise "floor" at about 2 MHz). As in the previous low-frequency measurement scheme,[52] a differential measurement is made using the two polarizations from the final polarizer to increase the signal to noise ratio. The photodiode loads are properly adjusted to maximize diode response at the modulation.

3. Time-domain Reflectrometry using the Electro-optic sampling technique

In general, the time-domain reflectrometer (TDR) consists of a step or impulse signal source, a directional coupler and a waveform acquisition device. An electrical waveform propagates from the pulse generator to the device under test (DUT), and the acquistion device detects the waveforms incident on and reflected from the DUT input for subsequent analysis. There are, however, several problems inherent in this implementation. For example, the measured waveforms differ from the true incident and reflected waveforms due to attenuation, dispersion and the time delay caused by the section of transmission line between the DUT and the plane of observation. In addition to correcting for these transmission-line effects, the effect of wafer probes, wirebonds, connectors, attenuators or other waveform-distorting elements which lie in the signal path must be de-embedded from the data. While it is desirable to locate the plane of observation of the sampling instrument at the DUT transmission-line interface to minimize these effects, the resulting temporal overlap of the incident and reflected waveforms makes it impossible to observe the DUT response. It is these problems that we address with the electro-optic approach.

In our specific implementation a coplanar waveguide and a photoconductive switch were fabricated using a lift-off process from 1500Å-thick gold on a semi-insulating <100> cut GaAs substrate. The lines were 3 cm in length with the switch positioned 1 cm from

one end of the waveguide as pictured schematically in Fig. 25. For simplicity, an open-circuit termination was substituted for the DUT.

The electro-optic waveform acquistion was performed as follows. A compressed picosecond pulse from a frequency-double YAG laser (λ = 530.2nm) was focused on to the 10 μm switch gap which was biased with a 100 kHz sine wave. The resulting optically generated carriers in the gap produced an electrical transient on the central waveguide conductor which propagated away from the switch on both directions on the waveguide. The electro-optic sampling was realized using the sub-bandgap (λ = 1.06μm) laser pulse to probe the electric field emanating from the central conductor of the waveguide. The signal was then processed by a signal averager and lock-in amplifier. Since the excitation and sampling laser pulses originated from the same source, they were precisely synchronized yielding jitter-free waveform acquisition.

As the symmetrically propagating pulses travel on the waveguide, they undergo equal degrees of attenuation and dispersion per unit distance given that the waveguide has uniform propagation characteristics over its length. Therefore, the waveform which arrives at point b in Fig. 25 will appear identical to the waveform arriving at point a, and by electrooptically sampling the waveform at point b, the waveform incident on the DUT is predicted. The reflected waveform is then obtained by subtracting the incident waveform from the waveform obtained at point a.

To test this concept we acquired the waveforms from our experimental set-up at a distance of 7mm on each side of the switch. As can be seen in Fig. 26 good agreement in the waveshapes was observed until the reflection from point a occurs at approximately 120 ps.

In contrast to the conventional TDR, the advantages of this approach can be enumerated as:

(i) Sampling is performed directly at the device/transmission line interface. As a result, de-embedding of the transmission line response is not required.

(ii) Device biasing may be applied on the end of the transmission line opposite the DUT, and, excluding wirebonds, no circuit elements lie in the signal path. allowing waveform acquisition with a low degree of distortion. For GaAs devices, transmission lines may be fabricated on a common substrate with the DUT, eliminated the need for direct wirebond connections to the DUT.

(iii) The photoconductive switching and electro-optic sampling approach to time-domain reflectometry allows generation and acquisition of subpicosecond rise-time waveforms. Experiments may thus be conducted with signal bandwidths exceeding 100 GHz.

4. Short Pulse Generation - J. Whitaker, M. Frankel, S. Gupta, G. Mourou (Rochester)

We present a technique for generating picosecond electrical pulses that does not rely on reducing carrier lifetime. We demonstrate this technique with semi-insulating GaAs, and it can be simply incorporated into any III-V semiconductor-based integrated circuits.

In transmission line structures discontinuities are usually detrimental since they distort the propagating signals. However, these signal-shaping properties can be used to

advantage. Specifically, inductive shunt and series capacitance discontinuities can produce pulses in response to step excitations. For our experiment, the transmission line used was a 50Ω Au/Ti coplanar waveguide on semi-insulating GaAs, with a 40 μm, centre conductor, 200 μm ground conductors and 25 μm conductor separation. A photoconductive switch gap was included in the centre conductor to generate the step excitation. The photoconductive switch, the signal-shaping discontinuity, and the waveguide terminations were each separated by 2 mm, providing a ~ 35 ps temporal measurement time window clear of reflections. The photoconductive switch was biased at 20 V.

The inductive shunt discontinuities, shown in Fig 27A, were incorporated into the structure as transverse segments connecting the central and outer conductors. Three different geometries were investigated to determine the influence of inductance on the signal characteristics: a 5 μm-wide meander line with a 10 μm loop size, a 5 μm-wide element and a 20 μm-wide element.

The series capacitance discontinuities were incorporated as gaps in the transmission line conductors. We investigated two structures, shown in Fig. 27(b): a ground line capacitor with a 10 μm straight gap, and an interdigitated capacitor in the centre conductor with a 5 μm gap, 10 μm fingers and two finger intervals. Fig. 27(a) shows a typical step-like excitation used as the input to the discontinuity measured 200 μm form the photoconductive switch The risetime of this waveform at the discontinuity is 2-8 ps. Fig. 27(a) also shows the measured signals 200μm after the inductive shunts, with geometrical details of the corresponding shunts. The negative afterpulse in these waveforms is due to a finite decay time of the incident excitations, and the ringing can be attributed to the parasitic capacitances present in the shunt discontinuity. The pulse duraction of 3 ps FWHM is nearly independent of the inductance, whereas the amplitude increases with increasing inductance. This behavior will be confirmed by the model presented later in this paper.

Fig. 27(b) shows the same excitation signal, as well as the signals 200 μm after the series capacitance discontinuities, with details of the corresponding discontinuity geometries. The discontinuity with the smaller capacitance shows pulse formation, whereas the one with larger capacitance does not. This is due to the fact that the large capacitance does not present a significant discontinuity for the propagating signal. Note that for a series capacitance the ringing is absent due to the negligible parasitic discontinuity inductances.

We have modelled the behavior of these discontinuity elements using lumped element analysis. If we assume an ideal step excitation with a risetime τ_{rise} and amplitude V_{in}, in maximum output pulse amplitude V_{out} and normalized duration τ_{fwhm} can be given as

$$V_{out} = V_{in}\, T(1-e^{-1/T}) \tag{8}$$

$$\tau_{fwhen} = T \ln [e^{1/T} + 1] \tag{9}$$

where the normalized time-constant is given by $T = 2Z_oC/\tau_{rise}$ for the capacitive discontinuity, $T = (2L/Z_o)/\tau_{rise}$ for the inductive discontinuity, Z_o is the waveguide characteristic impedance and C and L are the discontinuity capacitance and inductance, respectively.

From the equations we see that for small T the pulse amplitude increases linearly with T while the pulsewidth remains approximately unchanged, which agrees with Fig. 27(a). The limit of small T applies to all the investigated shunt inductances and the centre conductor interdigital capacitance. For large T, as in case of the ground conductor gap capacitance, the pulse amplitude approaches V_{in} while the pulsewidth increases, which explains the corresponding waveform of Fig. 27(b).

The values of the inductive discontinuity, when considered as finite length metal strip, can be estimated from Reference 56 and the values of capacitances can be estimated from Reference 57. These, as well as the values inferred from the experiment are summarized in Table 1. The close agreement between the calculated and epxerimental values indicates the applicability of the lumped element approach to the analysis of the discontinuity performance.

Table 1 Experimental and Calculated Valueds of Discontinuity Elements

Structure	L_{exp}	L_{cal}	C_{exp}	C_{cal}
	pH	pH	fF	fF
20 μm shunt	3•5	4	-	-
5 μm shunt	10	7	-	-
Meander shunt	22	14	-	-
Ground gap	-	-	75	80
Centre gap	-	-	4	4•3

In conclusion, we have demonstrated a simple and effective method for generating carrier lifetime independent picosecond electrical pulses. The minimum pulsewidth is determined primarily by the risetime of the incident excitation and thus there exists the possibility of subpicosecond pulse formation. Lumped element analysis provides a good reference point for the synthesis of the pulse-generating discontinuities.

B. Short Electrical Pulse Propagation - J. Whitaker, D. Dykaar, T. Hsiang, G. Mourou (Rochester)

The need to increase the speed of response of many systems and components has led to great advances in the field of ultrafast, very high frequency electronics. Novel devices operating in the millimeter-wavelength range[31,32] and new techniques for the generation and detection of electrical transients with terahertz bandwidth [33-36] have been designed. The progress in millimeter-wave integrated analog and digital circuits has led to the demand for a means to transmit waveforms of short duration from one location to another while maintaining fidelity. Since it has been discovered that it is difficult to propagate a signal with broad bandwidth on conventional striplines[37,38], it is necessary to investigate variations on the design of transmission structures - such as the use of superconducting striplines - and understand how these designs affect electrical signals. From the circuit point of view, it is desirable to have a design tool developed which is capable of modeling these new transmission lines.

We report results measured on indium (In) striplines. Our experiments made use of the cryogenic electro-optic sampler.[39,40]. This sampler has demonstrated time resolution of 360 fs, best among samplers reported to date. The experimental geometry is shown in Fig. 28. A gallium arsenide (GaAs) photoconductive switch was excited by 80 fs full width at half-maximum laser pulses and used to generate subpicosecond electrical transients that propagated on a pair of equally spaced striplines, 500 nm thick, 50 μm wide, and separated by 50 μm. This coplanar transmission line was continued onto a piece of 500-μm-thick $LiTaO_3$ crystal. A second laser beam was then used to probe the induced birefringence in the crystal. spatial resolution was achieved by directing the probing beam at different locations along the transmission lines. Typical sequences of the measured transients, below and above T_c, are shown in Figs. 29(a) and 30(a). A novel "pulse-sharpening" was observed immediately following the rising edge for propagation distances as long as 2 mm. All other dispersive characteristics discussed above were also seen. To analyze these results we use a procedure similar to that in Ref. 41 with the Mattis-Bardeen effect added in the consideration of conductivity.

Figure 31 shows the distribution of the fringing field lines for the coplanar geometry. Since part of the field lines line in helium ($\epsilon_{He} \cong 1$) and part in the substrate, an effective permittivity $\epsilon_{eff}(f)$ is used to describe the propagation speed at frequency f, as $v = c/\epsilon_{eff}^{1/2}(f)$, where c is the speed of electromagnetic radiation in free space. At low frequencies where transverse electromagnetic (TEM) mode propagation can be assumed,[41] a quasi-static analysis has been done to obtain the low-frequency permittivity $\epsilon_{eff}(0)$.[42] Full wave analyses are available to generate a closed-form expression for use at high frequencies when non-TEM modes are present.[43,44]

$$\sqrt{\epsilon_{eff}(f)} = \sqrt{\epsilon_{eff}(0)} + \frac{\sqrt{\epsilon_r} - \sqrt{\epsilon_{eff}(0)}}{1 + aF^{-b}}, \tag{10}$$

where ϵ_r is the permittivity of $LiTaO_3$, a and b are geometry dependent, dimensionless parameters which are set for use with a coplanar analysis, and $F = f/f_{TE}$ is normalized to the frequency f_{TE}, above which the first non-TEM mode enters in a microstrip. For our particular case $a \cong 23.5$, $b \cong 0.9$, and the cutoff frequency is found to be about 800 GHz.

Qualitatively, more of the fringing field lines lie in the dielectric at higher frequencies, leading to a form of $\epsilon_{eff}(f)$ that increases with frequency. Since this effect covers a wide range of frequency[41] (about 4 decades), the faster, low-frequency components in the signal will "catch up" with the high-frequency components and pulse distortion occurs, including the pulse sharpening effect if the conductor loss is small.

For a superconductor, the conductor loss is described by the Mattis-Bardeen expression $\sigma = \sigma_1 - i\sigma_2$, with σ_1 and σ_2 calculated from the weak-coupling theory.[4] In the case of normal lines, σ_1 is just the normal-state electrical conductivity σ_n, and σ_2 is zero.

An input transient, $v_{in}(\tau,0)$, equal to the time profile of voltage at the earliest measurement point ($z = 0$), can be Fourier transformed to yield an input spectrum $F\{v_{in}\}$, to which the propagation factor at each frequency, $\gamma(f)$, is applied. The distorted temporal signal $v_{out}(\tau,z)$ is then returned after an inverse Fourier transform:

$$v_{out}(\tau,z) = F^{-1}[F\{v_{in}\} \exp\{-\gamma(f)z\}]. \tag{11}$$

The propagation factor γ and the characteristic impedance Z_0 are related[45] to the series impedance Z and shunt admittance Y, per unit line, as $\gamma = \sqrt{ZY}$ and $Z_0 = \sqrt{Z/Y}$. Through substitution, it is seen that

$$\gamma = Z/Z_o(f)\,, \tag{12}$$

where

$$Z = i2\pi f\mu_0 g_1 + Z_s(f)g_2 \tag{13}$$

and g_1 and g_2 are functions dependent on the transmission line geometry and can be derived from design equations in Ref. 42. The first term in Eq. (13) is due to the inductive impedance, while the second, proportional to the conductivity through the surface impedance, Z_s, takes into account field penetration in the conductor (see, e.g., Ref. 43). Making use of the relation $Y = i2\pi f\epsilon_0\epsilon_{eff}/g_1$, $\gamma(f)$ is now calculated, recalling that frequency dependence may be derived from the effective permittivity and the Mattis-Bardeen conductivity. The detailed expressions of these functional dependences can be found elsewhere.[46,47]

By definition, the real part of the propagation factor, α, yields the attenuation of the line, while its imaginary part β produces the phase factor, from which the phase velocity is found to be $v_\phi = 2\pi f/\beta$.

Examining Eqs. (3) and (4) and neglecting dielectric loss, we have for γ

$$\gamma = \mathrm{Re}[\gamma]_{cond} + i\,\mathrm{Im}[\gamma]_{cond} + i\,\mathrm{Im}[\gamma]_{modal}, \tag{14}$$

where

$$\alpha_{cond} \equiv \mathrm{Re}[\gamma]_{cond} - \mathrm{Re}[Z_s/Z_0(f)]g_2 \tag{15}$$

and

$$\beta_{cond} \equiv \mathrm{Im}[\gamma]_{cond} = \mathrm{Im}[Z_s/Z_0(f)]g_2 \tag{16}$$

and the last term reduces to

$$\beta_{modal} \equiv \mathrm{Im}[\gamma]_{modal} = (2\pi f/c)\sqrt{\epsilon_{eff}(f)}. \tag{17}$$

The equations above show that the complex surface impedance always influences the attenuation and phase factors of a transmission line. For a normal line, β_{modal} is much greater than β_{cond}; it is only when the superconducting energy gap is approached that β_{cond} becomes important, adding to β_{modal} to cause increase dispersion. That is, below the energy gap, the propagation phase velocity decreases with increasing frequency in a fashion similar to that for the modal dispersion effect.

Using the first detected signal ($z = 0$) as the input, a code was generated from the algorithm described above to compute the sequential output signals at various propagation lengths. The results are shown in Figs. 29(b) and 30(b) for superconducting and normal cases respectively, where it is seen that *all* of the experimentally observed features are reproduced by the computation.

The experimental results *cannot* be simply attributed to the effect of superconducting complex conductivity alone as demonstrated in Fig. 29(c), where we show the computed results for the superconducting lines that neglected the β_{modal} factor. In this case, the distortion is significantly underestimated by the computation. On the other

hand, the close resemblance between the superconducting and normal results [in Figs. 29(a) and 30(a)] indicates that modal dispersion is the dominant effect, until propagation length and conductor loss become significant.

A final point to note is that, in obtaining the waveforms in Figs. 29 and 30, we have used an experimentally determined value (from time delay measurements of transients propagated over different distances) of $\epsilon_{ff}(0) \approx 10$. This leads to a calculated value for high-frequency effective permittivity[42] of approximately 20. This latter number corresponds to about half the static permittivity of LiTaO3($\epsilon_r \approx 43$), and this indicates that the ϵ_r term in Eq. (1) probably should be replaced by $\epsilon_{ff}(\infty)$ for coplanar striplines to represent the high-frequency effective permittivity. While this conjecture appears reasonable physically, we do recognize that it somewhat contradicts the results of Ref. 44, although the differences may be accounted for in some of this reference's fitting techniques.

In conclusion, we have presented experimental results and theory on the propagation characteristics of picosecond electrical transients on coplanar transmission lines. We showed that, in order to describe all of the experimental observations, both the effects of modal dispersion and superconducting complex conductivity must be taken into account. An algorithm has been outlined for accurately describing the picosecond transient propagation in both superconducting and normal lines.

C. Picosecond Reflection High-Energy Electron Diffraction (RHEED) - H. Elsayed-Ali, G. Mourou, S. Williamson, R.S. Knox, Hsiu-Chen (Rochester)

The study of surface phase transitions and reactions is a rapidly maturing science from both theoretical and experimental points of view. The advancement of such knowledge, however, requires the development of a direct time-resolved surface structural probe capable of monitoring the complex processes of surface phase transisitons and reactions. We report on the demonstration of reflection high-energy electron diffraction (RHEED) with photogenerated picosecond electron pulses. Due to the synchronization of the electron pulses with the laser source, such as technique provides a picosecond time-resolved surface structural probe.

Electron diffraction (both high energy and low energy) provides a "natural" surface probe that is well developed and has been utilized for many decades in surface studies. Construction of a picosecond transmission electron diffraction apparatus was accomplished a few years ago.[58] This technique was applied to study the dynamics of laser melting of free-standing thin aluminum films.[59] Subsequently, a nanosecond low-energy electron diffraction (LEED) apparatus was developed and utilized in surface temperature measurement during laser annealing of germanium.[60] In such a setup, due to the low electron energy, space-charge effects severely limited the ability to observe the diffraction pattern. It was estimated that, on the average, only one electron per shot was reflected from the surface.[60] Thus, averaging over a very large number of shots was required in order to obtain meaningful data. This limitation precluded the use of this technique to study nonrecurring surface structural phenomena. In contrast, due to the much less severe space-charge limitations in picosecond RHEED, we have demonstrated that excellent quality

surface diffraction patterns could be obtained with a total exposure time on the order of 100 ps.

The picosecond electron diffraction system, is a modification of the previously described system.[58,59] The photocathode was ~250 Å gold film deposited on a sapphire window by conventional evaporation technique. Such a photocathode was rugged enough to withstand months of operation with repeated exposure to the atmosphere. A circular aperture of 0.25 mm diameter located 1 mm form the photocathode was used as an extraction electrode. The extraction electrode was followed by a focus electrode and an anode which was located 140 mm from the photocathode. The specimen was mounted on a manipulator providing linear motion, rotation, and tilt. The diffraction pattern was amplified by a microchannel plate and observed using a P-47 phosphor screen deposited on a fiber-optics faceplate which provides near to zero distortion of the diffraction pattern. The system was typically operated at a pressure of ~2 x 10^{-6} Torr.

The photocathode was activated by ultraviolet light from a frequency quadrupled Nd:yttrium aluminum garnet (YAG) regenerative amplifier (an injection-locked multipass amplifier[61]). This system provided ~0.4mJ pulses at 1.06 μm and a pulse width of 120-160 ps. The repetition rate of the regenerative amplifier could be varied form a single shot to 1.5 kHz with shot-to-shot stability better than 5%. Only a very small fraction of the output of the regenerative amplifier was frequently quadrupled (<10^{-3}); thus the 1.06μm fundamental wavelength contained almost all the energy and could be utilized for sample heating. The frequency quadrupled Nd:YAG (λ = 0.266μm) was incident normal to the photocathode and had ~0.1 mm spot size diameter on it. The electron replica of the UV pulse, generated at the photocathode, was swept by the extraction aperture and further accelerated and focused in the focus electrode to a focal spot of ~ 0.8 mm on the phosphor screen. These electrons were incident in a grazing angle on the surface of the specimen and Bragg diffracted giving a RHEED pattern.

Figure 32 shows a RHEED pattern of a cleaved surface of a sodium chloride crystal obtained using a single electron pulse and after averaging 50 pulses. The electron energy was 25 keV and a field of 23 kV/cm was applied between the photocathode and the extraction electrode. Although the number of electrons per pulse, measured by a Faraday cup and a picoammeter, was found to be directly proportional to the UV intensity on the photocathode, space-charge-induced temporal broadening of the electron pulse with increased UV intensity was observed. Measurements of the electron pulse width were accomplished by operating the diffraction system as a streak camera with the streak voltage supplied by a laser activated Cr:GaAs photoconductive switch.[62,63] For conditions used in Fig. 32 the electron pulse width used to obtain a RHEED pattern was measured to be ~200 ps. The number of electrons delivered to the specimen per pulse was ~ 5 x 10^5. As seen form Fig. 27(a), good RHEED patterns could be obtained even with a single electron pulse. This makes the study of nonrecurrent events possible. Better quality diffraction patterns could be established by averaging several pulses as shown in Fig. 27(a). Extension of the present technique to a few picoseconds, or even subpicosecond, resolution should be possible by pulse compression of the driving laser and by minimization of electron temporal broadening.[64,65]

For studying recurrent events, it would be advantageous to operate the picosecond RHEED system at a high repetition rate. The persistence time (decay time to 10% peak value) of the P-47 phosphor is 0.15μs. Thus, megahertz operation is possible using a

continuous mode-locked laser as a driver The primary limitation on repetition rate in the present system is due to microchannel plate "dead time"[66] (time needed to replenish the charge in the channel wall). This depends on operating conditions and typically allows kilohertz operation. With increased exposure time, however, the microchannel plate amplification stage could be removed.

In summary, we have demonstrated the technique of picosecond time-resolved reflection high-energy electron diffraction. This technique represents a direct time-resolved surface structural probe limited to the first few monolayers and synchronized with the driving laser source. Application of this technique could include the study of surface structural and chemical changes. We are currently constructing a picosecond RHEED system operating in ultrahigh vacuum. Future experiments will include the study of surface phase transformations and chemical reactions.

We have performed measurements of the surface Debye-Waller effect with a few hundred picoseconds time resolution on a Pb(110) crystal. The system was operated at 8 Hz repetition rate. The laser heating pulse, which was incident normal to the sample, had an energy of 15-16mJ with a spot size of ~1.2 cm FWHM (sample diameter 1.1 cm).

The time-resolved results were related to the lattice temperature by observing the diffraction intensity changes under static heating conditions and comparing with the intensity changes due to laser heating. The validity of this temperature calibration was not directly tested. However, this calibration should hold for time scales longer than that needed for equilibrium to be established between the electrons and the lattice. In metals, at room temperature or higher, this typically occurs within a few picosecond.[67]

Results for two different experimental runs are shown in Fig. 33 along with the decay of the surface temperature rise obtained from a heat diffusion model[68]

$$C[dT(z,t)/dt] = K[d^2T(z,t)/dz^2] + I(1-R)\,\alpha e^{-\alpha z} f(t). \qquad (18)$$

where C is the heat capacity per unit volume, T(z,t) is the temperature profile at distance z normal to the sample surface, t is time, K is the thermal conductivity, I is the laser peak intensity, α is the absorption per unit length, and f(t) is the time dependence of the laser pulse which is assumed Gaussian with e^{-1} full width of 420 ps (based on a streak camera measurement).

The surface temperature rise obtained using the transient surface Debye-Waller effect on the picosecond RHEED pattern shows general agreement with that predicted by a heat diffusion model (Fig.33). An uncertainty in the model, however, is the value of the reflectivity and absorptivity for which we relied on published results for the complex index of refraction. Nonlocal effects on the thermal conductivity which arise if the temperature gradient is significant within a mean free path of the heat carriers,[69] i.e., hot electrons, were not included. Such nonlocal effects were shown to reduce heat conductivity.[69]

We have demonstrated the use of picosecond RHEED as a time-resolved surface temperature probe. The temperature measurement is based on the surface Debye-Waller effect which results in a reduction of the number of elastically scattered electrons with lattice heating. Time-resolved measurements of the picosecond laser heated Pb(110) surface showed general agreement with a heat diffusion model.

The technique of picosecond RHEED offers both surface selectivity and temperature sensitivity. In addition to its utilization as a time-resolved structural and

temperature probe of fast surface processes, it can also be used to study the thermal properties of extremely thin films (up to a few monolayers).

III. Ultrafast Devices

A. Picosecond Photoconductive Detector - S. Gupta, M. Frankel, D. Dykaar, G. Mourou, and T. Hsiang (Rochester)

We report here the development of a GaAs-based highspeed photoconductive detector that overcomes the limitations cited above. The measured speed of the current device is approximately .5ps (full width at half maximum, FWHM) and the response is of the order of a volt using a bias of 10 V and an 80 fs laser pulse of 90 pJ energy. The material appears to be stable for indefinite periods of time. Further, the switch can be easily integrated with GaAs discrete devices and circuits. In fact, the material that is used for this device also offers profound performance improvements for GaAs devices and ICs.[80,81]

The active layer of the photoconductive detector is deposited by molecular beam epitaxy (MBE) using Ga and As_4 beam fluxes at a substrate temperature of 200°C. This temperature is substantially lower than that usually used to deposit high quality conducting films of GaAs by MBE, 560-600°C. The low-temperature (LT) GaAs was deposited at a growth rate of 1 μm/h, under arsenic stable growth conditions. These films of LT GaAs have both electrical and optical properties that are markedly different from GaAs grown at 580°C [80,81] Although the LT GaAs is crystalline as demonstrated by x-ray diffraction and transmitted electron diffraction measurements,[82] it has a resistivity that is substantially greater than that of semi-insulating GaAs ($\rho_{LTGaAS} > 10^7$d cm). Further, the LT GaAs exhibits virtually no photoluminescence.[80-82] The increase in resistivity is consistent with a dramatic increase in the deep level concentration in the film as the substrate temperature is reduced, but deep levels alone would not explain a resistivity substantially greater than that of semi-insulating GaAs. The abnormally high resistivity has so far precluded measurements of carrier mobility. The resistivity increase appears to be associated with excess arsenic incorporated into the LT GaAs grown at 200°C is highly nonstoichiometric; the LT GaAs is approximately 50.2% As and 49.5% Ga.[89]

Short photoexcited-carrier lifetime, coupled with high carrier mobility, are the desired characteristics for a highspeed photoconductive switch. Transmission electron microscopy studies indicate that the dislocation density in LT GaAs is as low as that seen in GaAs epitaxial layers grown at normal substrate temperatures.[83] The crystal perfection can lead to a high mobility, while a high deep level density can lead to short recombination lifetimes. Also, the measured dielectric-breakdown field of LT GaAs is in excess of 3 x 10^5 V/cm, so that LT GaAs photoconductive switches should support high-voltage electrical impulses.

The ultimate speed of a LT GaAs photoconductive detector was measured using a photoconductive-gap switch with a coplanar transmission line and the technique of electro-optic sampling. The switch is formed on a 50 μm coplanar strip transmission line having a characteristic impedance of 91Ω. A 20 μm tapered gap was incorporated into one of the two legs of the transmission line. The electrodes are indium metal and a 10 V square-wave signal at 3.7 MHz was applied across the input side of the transmission line.

A probe beam consisting of ~80 fs laser pulses at a 100 MHz repetition rate with a wavelength of 620 nm and an average power of ~9 mV (90 pJ/pulse) was focused onto the 20 μm gap. The electrical pulse generated by this optical pulse was sampled. The electrical signals measured is shown in Fig. 34(a). The FWHM of the pulse approximately 0.5ps. This result translates into a 3 dB bandwidth of around 600 GHz. The measured maximum voltage of the impulse is ~0.4 V, for a pulse energy of 90 pJ and 10 V bias across the transmission line. The 0.5ps result is comparable with the highest speeds ever reported for a photoconductive switch and the measured sensitivity is over an order of magnitude greater than that which we have measured for switches based on damaged materials or oxygen-implanted SOS.

In conclusion, we have fabricated a photoconductive detector using LT GaAs grown by MBE at a temperature of 200°C. Autocorrelation measurements of the detector yielded a system limited response of ~7.5 ps. Electro-optic sampling was used to measure a temporal response of ~0.5ps FWHM and an amplitude of ~0.4 V for a 10 V bias. These results compare favorably to the best results for any photoconductive switch yet reported. Further, devices used in this study were fabricated on material that was grown by MBE over one year ago and as recently as one month prior to testing, and, hence, the LT GaAs appears to be stable for extended periods of time. By optimizing this device, it may be possible to achieve even greater speeds and/or sensitivity. Since LT GaAs is compatible with GaAs device and IC technologies, this photoconductive switch could find extensive use in high-speed device and circuit testing.

B. >100 GHz Electro-optic Modulator - J. Nees, S. Williamson, G. Mourou (Rochester)

Signal processing, optical communication, and computer technology require a broadband modulator with low operating power. The optical waveguide, due to the confinement of the optical beam over a long distance, makes optical modulation with long interaction length possible[70-75]. The driving power for a traveling wave modulator, of impedance Z_o, is given by the expression

$$P = \left[\frac{d}{l}\left(\frac{\lambda}{n^3 r}\right)\right]^2 / Z_o \qquad (19)$$

where n is the index of refraction, l the wavelength in free space, r is the effective electro optic coefficient, d is an effective electrode separation, and l is the waveguide length.

The modulator bandwidth is determined on one hand by the dispersive properties of the transmission line due to modal dispersion[76], and skin effect losses[77], and, on the other hand, by the phase velocity difference[78] between the optical and electrical waves. It is the velocity mismatch which is presently limiting the time response of the traveling wave modulator to 20 GHz.

To minimize modal dispersion, it is necessary to use transmission lines with small cross sectional dimensions. Due to the air-substrate interface, quasi-TEM propagation occurs only when the cross-sectional dimensions of the transmission lines are small

compared to the wavelength of the driving signal. For coplanar lines, the effective dielectric constant is frequency dependent as shown in Fig. 35. The cut-off frequency ν_c, of the surface wave TE_1 mode[79] follows the form

$$\nu_c \sim \frac{c}{4d\sqrt{\varepsilon_{sub} - \varepsilon_{sup}}} \tag{19}$$

where c is the speed of light and the dielectric constant of the substrate, ε_{sub}, is greater than the dielectric constant of the superstrate,ε_{sup}.

Contrary to modal dispersion, skin effect losses demand electrode dimensions to be as large as possible. Consequently, for high frequency operation, modal dispersion and skin effect losses are irreconcilable. We will see later, than in order to avoid modal dispersion and skin effect simultaneously, it is necessary to use superconducting electrodes. Figures 36(a) and 36(b) illustrate the effects of modal dispersion and skin effect losses on the short electrical pulse propagation. The two figures are the result of computer simulation. Figure 36(a) shows the broadening of a 1 ps rise time step function after 10 mm propagation on a gold coplanar transmission line evaporated onto a GaAs substrate. The width and electrode separation are both 20 μm. It can be seen after 10 mm, the rise time has degraded from an initial value of 1 ps to 5 ps. In Fig. 36(b), the modal dispersion has been turned off and the observed decrease in rise time and signal amplitude are due solely to the skin effect attenuation.

As mentioned earlier, the most important mechanism limiting the speed of the electrooptic modulator is the velocity mismatch between the optical and electrical signals. This effect limits the rise time τ_r of the modulator to a value

$$\tau_r = \Delta n \bullet \frac{l}{c} \tag{20}$$

where $\Delta n = \sqrt{\varepsilon_{eff}}$ - n and n is the substrate index of refraction.

By placing a GaAs superstrate in contact with a GaAs/GaAlAs waveguide, the condition $\sqrt{\varepsilon_{eff}} = n$ can be satisfied. This enables us, for the first time, to suppress the effect of the velocity mismatch in longer, more efficient modulators.

A diagram depicting this modulator is shown in Fig. 37. A waveguide was prepared on a GaAs substrate. Vertical confinement was provided by a series of MBE grown GaAlAs layers and horizontal confinement by a ridge etched in the upper layer. The coplanar striplines were 100 μm wide and separated by 20 μm. The film is gold of 5000 Å thickness. A 10 μm photoconductive switch interrupted one line; 0.5 mm from the modulator's input end. The resistance of the metalization over the 5 mm modulator length was 7.5 Ω. The GaAs superstrate was then placed in contact with the coplanar transmission lines.

After passing through a quarter-wave plate about 10% of the compressed IR light from a Nd:YAG laser was coupled into a 4 μm core fiber 40 cm in length. This fiber was then butt coupled to the input of the modulator waveguide. A 20X microscope objective was used at the output to image the modulated light through a polarizer and onto a reverse

biased PIN photodiode. The remaining 90% of the compressed IR beam was converted to 532 nm at 2% efficiency in KTP to form the switch pump pulse. The green light was first chopped at the lock-in reference frequency of 4 MHz by an acousto-optic modulator and passed through an optical delay line to allow adjustment of pump/prove timing. Finally, the pump pulse was focused onto the photoconductive switch. A step function electrical pulse was generated and the rise time measured by the short probe pulses which correspond directly to the response time of the modulator as it would be used with cw optical input. The result of modulating with a subpicosecond step function and a 1 ps probe pulse is shown in Fig. 38. The 10%-90% rise time is found to be 3.2 ps. If a Gaussian rising edge is assumed, this rise time corresponds to 110 GHz for 3dB roll-off.

A measurement of the half-wave voltage of this modulator at 4 MHz yielded a value of 288 V. This is nearly a factor of 4 above the expected value of 75 V. The loss in sensitivity was probably due to depolarization of the modulated beam in the input fiber.

As more devices begin to function at frequencies above 100 GHz and as the demand for test equipment increases, the need for an ultrafast modulator will continue to grow. We have demonstrated a GaAs modulator with velocities nearly matched. This is simply achieved by putting a GaAs superstrate in contact of a GaAs waveguide. Further improvement can be achieved by varying the aluminum mole fraction in a GaAlAs superstrate. This approach should make the construction of 500 GHz possible with lower half-wave voltage. At these frequencies, the skin effect losses will become dominant and superconducting electrodes will have to be used. The superconducting electrodes will have to possess a large energy gap in excess of 0.5 THz. Superconductors such as Nb with a T_c = 9°K and an energy gap corresponding to 700 GHz could be used. High T_c superconductors with an energy gap corresponding to 10 THz could even be a better choice. Recent experiments have shown that picosecond electrical pulses could propagate over distances of 1 cm on high T_c superconducting lines without detectable absorption or dispersion. Furthermore, the dielectric constants of some high T_c substrates nearly match that of GaAs.

IV. Laser Technology

A. Femtosecond Pulse Amplification - P. Bado, S. Coe, J. Squier, D. Strickland, G. Mourou and M. Pessot (Rochester)

The advent of chirped-pulse amplification[85] had led to a renewed interest in the development of solid-state amplifiers for ultrashort pulses. The broad bandwidth and high energy-storage capabilities of solid state materials such as alexandrite and Ti:sapphire point to the potential for these materials in the production of high-energy femtosecond pulses. Recently, the generation of 300-fsec pulses at the millijoule levels in an alexandrite regenerative amplifier[86] was reported.

We have showed that this limitation can be overcome by using a combination of diffraction gratings in conjunction with a sequence of prisms[87] to compensate for both the quadratic and cubic phase shifts arising form the dispersive elements. In this way we are able to generate pulses as short as 106 fsec with peak powers of ~20 GW.

The basic system used here is similar to that of Ref. 86, although some modifications have been made. First, the dye laser used in these experiments (765 nm, 300 fsec) does not provide a short enough pulse. In order to provide sufficient bandwidth for the generation of 100-fsec pulses, the dye-laser output was amplified in a conventional dye amplifier and coupled into a 20-cm-long section of polarization-preserving, single-mode fiber. The spectrum could be broadened out to ~25nm through self-phase modulation within the fiber,[88] with the pulse width broadening to ~1 psec. The pulse was then preamplified and double passed through a grating expander before it was injected into an alexandrite regenerative amplifier. Grating expansion has been shown to easily provide sufficient dispersion to broaden femtosecond pulses by a factor dispersion to broaden femtosecond pulses by a factor of 10^2-10^3.[86,89] The grating expander was identical to that used previously,[86] consisting of two antiparallel 1800-line/mm gratings separated by 145 cm. with a pair of 500-mm lenses between the gratings forming a unit magnification telescope. The injected energy was typically in the 5-10-nJ range in a pulse ~120 psec long.

The contrast previous research in which the spectrum of the input pulse was significantly narrower (~3 nm), the spectrum of the amplified pulse from the alexandrite regenerative amplifier was found to be sensitive to any mismatch between the peak gain of the alexandrite (~760 nm) and the operating wavelength of the dye laser. When the dye-laser operating wavelength was ~3.5 nm to the red of the amplifier gain center, a severe spectral narrowing and reshaping of the self-phase-modulated input spectrum was observed. Broad spectra were narrowed considerably, from 23 to 8 nm, after amplification to an energy of only ~100 μJ, with the red side of the spectrum being completely depleted.

In order to match the dye/amplifier wavelengths precisely, the alexandrite rod was run at an elevated temperature or 150°C. Alexandrite is known to have a temperature-dependent emission cross section that shifts to longer wavelengths at higher temperatures.[88] This was preferred to insertion of any bandwidth-limiting tuning elements in either the dye laser or alexandrite amplifier to bring the two into resonance. With the wavelengths matched to within 1 nm, the spectral reshaping is reduced substantially. The spectrum of the amplified pulse has narrowed only slightly, to 12 nm. This residual narrowing seems to be a true spectral narrowing, as broader input spectra were also narrowed in this situation to approximately the same width. The observed spectral narrowing can arise form the frequency-dependent cross section of the material and/or any other optical component with a wavelength dependence. The observed output is approximately half of the expected effective bandwidth for an alexandrite amplifier with a fluorescence bandwidth of 1800 cm^{-1}(Ref. 89) and a gain of 10 [87,90] indicated that other cavity components may also be contributing to the observed spectral reshaping.

The presence of dispersive material elements within the regenerative amplifier cavity leads to a further broadening of the input pulse and to limitations on the maximum compression that can be achieved. This limitation arises form the need to adjust the compression-grating separation to compensate for the dispersion accumulated during the 50-55 round trips that the pulse makes within the cavity. Adjustment of the compression-grating separation to compensate for both the expansion gratings and the accumulated linear dispersion from the material elements results in a substantial residual quadratic dispersion that limits the compressed pulse width. We wish to stress that the bulk of the residual (quadratic) dispersions not contributed by the material elements but form the gratings. It is

a consequence of not using the expansion and compression gratings at identical effective separations and angles of incidence. The expansion/compression gratings are then no longer matched dispersive devices and make a contribution to the residual dispersion that is approximately three times the contribution from the material elements. In Ref. 86 it was shown that the residual dispersion would limit the pulse width to ~200 fsec.

We have modified our alexandrite regenerative amplifier to incorporate a prism sequence to provide the necessary higher-order compensation Fig. 39. We have place four Brewster-angled prisms of SF-10 glass within the cavity with a separation of 43 cm. Two of the prisms were placed on stages so that the prism could be translated in a direction perpendicular to its base. Placing the prisms internal to the cavity allows us to take advantage of the large number of transits that the pulse makes to accumulate the required amount of compensation. External to the cavity the required prism spacing was not feasible.

The prism separation was chosen on the basis of calculations of the contributed phase shift from all dispersive elements both internal and external to the cavity. The prism and grating separations were used as the two degrees of freedom to find some point at which the quadratic and cubic phase shifts would cancel. Strictly, this cancellation holds only for a unique number of transits within the cavity. This could be controlled by varying the level of the signal injected into the cavity and setting the cavity dumper to fire at a specific time interval after the Q-switch, rather than cavity dumping on the basis of a threshold detectors' monitoring the energy buildup of the pulse. With the prism sequence included, the compression gratings were then varied to optimize the compressed pulse. Further optimization should have been possible by translating the prisms into the beam path. In practice, it was found that mechanical instabilities prevented us from making significant translations of the prisms.

Single-shot, background-free autocorrelation[91] measurements were used to monitor the compressed pulse width. Figure 40 shows a 106-fsec pulse, assuming a $sech^2$ pulse shape for deconvolution. The 40% (double-pass) diffraction efficiency of the gratings reduced the pulse energy from 5 to 2 mJ, which yielded a peak power of almost 20 GW. When the prism sequence was not included within the cavity, the shortest compressed pulse observed was 170 fsec. This is in reasonable agreement with the minimum width expected form the limitations described above, indicating that we have achieved a partial cancellation of the cubic phase. We believe that the incomplete compensation is a result of a mismatch of a few degrees in the angle of incidence of the beam between the expansion and compression-grating stages, resulting in a large cubic phase than our design could compensate. The overall expansion/compression ratio of over 1100 is comparable with that seen in multiple-stage fiber-grating compression systems.[91,92]

In summary, we have shown that chirped-pulse amplification techniques can be used for the production of amplified femtosecond optical pulses from broadband solid-state systems. We have demonstrated that a combination of intracavity prisms and diffraction gratings can be used to provide compensation of cubic phase shifts, circumventing limitations in the compressed pulse width that arise from dispersive elements within the cavity. Simple extensions of the results shown here indicate the potential of chirped-pulse amplification for the production of terawatt femtosecond pulses in the near future.

FOOTNOTES

1. G. Mourou, K. Meyer, J. Whitaker, M. Pessot, R. Grondin, and C. Caruso, in *Picosecond Electronics and Optoelectronics II*, Spring Series in Electronics and Photonics 24, 40 (1987).
2. M. Osman and H. Grubin, *Solid-State Electron.* 31, 471 (1988).
3. R. O. Grondin and M. J. Kann, *Solid-State Electron.* 31, 567 (1988).
4. A. Evan Iverson, G. M. Wysin, D. L. Smith, and A. Redondo, *Appl. Phys. Lett.* 52, 2148 (1988).
5. G. M. Wysin, D. L. Smith, and A. Redondo (unpublished).
6. G. A. Mourou and K. E. Meyer, *Appl. Phys. Lett.* 45, 492 (1984).
7. H. C. Liu and D. D. Coon, *Appl. Phys. Lett.* 50, 1246 (1987).
8. W. D. Goodhue, T. C. L. G. Sollner, H. W. Le, E. R. Brown, and B. A. Vojak, *Appl. Phys. Lett.* 49, 1086 (1986).
9. J. A. Valdmanis, G. A. Mourou, and C. W. Gabel, *IEEE J. Quantum Electron.* QE-19, 664 (1983).
10. D. D. Coon and H. C. Liu, *Appl. Phys. Lett.* 49, 94 (1986).
11. M. Tsuchiya, T. Matsusue, and H. Sakaki, *Phys. Rev. Lett.* 59, 2356 (1987).
12. E. O. Göbel, H. Jung, J. Kuhl, and K. Ploog, *Phys. Rev. Lett.* 51, 1588 (1983).
13. J. F. Ryan, R. A. Taylor, A. J. Turberfield, A. Maciel, J. M. Warlock, A. C. Gossard, and W. Wiegmann, *Phys. Rev. Lett.* 53, 1841 (1984).
14. J. E. Fouquet and R. D. Burnham, *IEEE J. Quantum Electron.* QE-22, 1799 (1986).
15. L. D. Landau and E. M. Lifshitz, *Quantum Mechanics, Non-Relativistic Theory*, 3rd ed. (Pergamon, New York, 1977), pp. 178-181.
16. J. Wei Wu and A. V. Nurmikko, *Phys. Rev. B* 37, 2711 (1988).
17. E. J. Austin and M. Jaros, *Appl. Phys. Lett.* 47, 274 (1985).
18. G. Wicks (private communication).
19 A similar structure has been independently proposed by S. Luryi, *Solid State Commun.* 65, 787 (1988).
20. D. A. B. Miller, D. S. Chemla, T. C. Damen, A. C. Gossard, W. Wiegmann, T. H. Wood, and C. A. Burrus, *Phys. Rev. Lett.* 53, 2173(1984).
21. C. Albert, S. Gaillard, A. Brun, G. Bastard, P. Frijlink, and M. Erman, *Solid State Commun.* 53, 457 (1985).
22. E. J. Auston and M. Jaros, *Appl. Phys. Lett.* 47, 274 (1985).
23. S. I. Anisimov, B. L. Kapeliovich, and T. L. Perel'man, *Zh. Eksp Teor. Fiz.* 66, 776 (1974) [Sov., Phys. JETP 39, 375 (1975)].
24. *American Institute of Physics Handbook*, edited by D. E. Gray (McGraw-Hill, New York, 1972), 3rd ed.
25. M. I. Kaganov, I. M. Lifshitz, and L. V. Tanatarov, *Zh. Eksp. Teor. Fiz.* 31, 232 (1956) [Sov. Phys. JETP 4, 173 (1957)].
26. D. K. Lathrop, S. E. Russek, and R. A. Buhrman, *Appl. Phys. Lett.* 51, 1554 (1987) and references therein.
27. S. Sridhar, C. A. Shiffman, and H. Hamdeh, *Phys. Rev. B* 36, 2301 (1987).
28. L. Cohen, I. R. Gray, A. Porch, and J. R. Waldram, *J. Phys.* F17, L179 (1987).
29. D. Grischkowski and I. N. Duling III, OSA meeting, Rochester, NY, 1987.
30. T. Y. Hsiang, J. F. Whitaker, R. Sobolewski, D. R. Dykaar, and G. A. Mourou, *Appl. Phys. Lett.* 51, 1551 (1987).
31. J. Pustai, "Millimeter-wave transistors: The key to advances systems," *Microwaves and RF* 26, no. 3, pp. 125-176, 1987.
32. K. E. Meyer, D. R. Dykaar, and G. A. Mourou, "Characterization of TEGFETs and MESFETs using the electro-optic sampling technique," *in Picosecond Electronics and Optoelectronics*, G. A. Mourou, D. M. Bloom, and C.-H. Lee, Eds. Berlin: Springer-Verlag, 1985, pp. 54-57.

33. G. A. Mourou and K. E. Meyer, "Subpicosecond electro-optic sampling using coplanar strip transmission lines," *Appl. Phys. Lett.* 45, pp. 492-494, Sept. 1984.
34. D. R. Dykaar, R. Sobolewski, J. F. Whitaker, T. Y. Hsiang, G. A. Mourou, M. A. Hollis, B. J. Clifton, K. B. Nichols, C. O. Bozler, and R. A. Murphy, "Picosecond characterization of ultrafast phenomena: New devices and new techniques," in *Ultrafast Phenomena V*, G. R. Fleming and A. E. Siegman, Eds. Berlin: Springer-Verlag, 1986, pp. 103-106.
35. D. R. Dykaar, R. Sobolewski, T. Y. Hsiang, and G. A. Mourou, "Response of a Josephson junction to a stepped voltage pulse," *IEEE Trans. Magn* MAG-23, pp. 767-770, Mar. 1987.
36. M. B. Ketchen, D. Grischkowsky, T. C. Chen, C.-C. Chi, I. N. Duling III, N. J. Halas, J.-M. Halbout, J. A. Kash, and G. P. Li, "Generation of subpicosecond electrical pulses on coplanar transmission lines," *Appl. Phys. Lett.* 48, pp. 751-753, Mar. 1986.
37. J. A. Valdmanis and G. Mourou, "Subpicosecond electrical sampling and applications," in *Picosecond Optoelectronic Devices*, C.-H. Lee, Ed. New York: Academic Press, 1984.
38. J. F. Whitaker, T. B. Norris, G. A. Mourou, and T. Y. Hsiang, "Pulse dispersion and shaping in microstrip lines," *IEEE Trans. Microwave Theory Tech.* MTT-35, pp. 41-47, Jan. 1987.
39. D. R. Dykaar, T. Y. Hsiang, and G. A. Mourou, *IEEE Trans. Magn.* MAG-21, 230 (1985).
40. D. R. Dykaar, R. Sobolewski, T. Y. Hsiang, and G. A. Mourou, *IEEE Trans. Magn.* MAG-23, 767 (1987).
41. J. F. Whitaker, T. B. Norris, G. A. Mourou, and T. Y. Hsiang, *IEEE Trans. Microwave Theory Tech.* MTT-35, 41 (1987).
42. K. C. Gupta, R. Garg, and I. J. Bahl, *Microstrip Lines and Slotlines* (Artech House, Deham, MA, 1979)
43. E. Yamashita, K. Atsuki, and T. Ueda, IEEE Trans. Microwave Theory Tech. MTT-27, 1036 (1979).
44. G. Hasnain, A. Dienes, and J. R. Whinnery, *IEEE Trans. Microwave Theory Tech.* MTT-34, 738 (1986).
45. R. E. Matick, *Transmission Lines for Digital and Communications Network* (McGraw-Hill, New York, 1969), Chaps. 4 and 6.
46. R. L. Kautz, *J. Appl. Phys.* 49, 308 (1978).
47. J. F. Whitaker, R. Sobolewski, D. R. Dykaar, T. Y. Hsiang, and G. A. Mourou, to appear in *IEEE Trans. Microwave Theory Tech.*, special issue on CAD, Feb. 1988.
48. J. Nees and G. Mourou, *Electron. Lett.* 22, 918 (1986).
49. J. A. Valdmanis and S. S. Pei, *Picosecond Optics and Electronics II*, F. J. Leonberger, C. H. Lee, F. Capasso, and H. Morkoc, Eds. (Berlin: Springer-Verlag, 1987).
50. K. J. Weingarten, M. J. W. Rodwell and D. M. Bloom, *IEEE J. Quantum Electron.* 24, 198, (1988).
51. G. Mourou, K. Meyer, J. Whitaker, M. Pessot, R. Grondin, and C. Caruso, *Picosecond Optics and Electronics II*, F. J. Leonberger, C. H. Lee, F. Capasso, and H. Morkoc, Eds. (Berlin: Springer-Verlag, 1987).
52. J.A. Valdmanis, G.A. Mourou, and C.W. Gabel, "Picosecond Electro-optic Sampling System", *Appl. Phys. Lett.* 41:211 (1982); see also J.A. Valdmanis and G.A. Mourou, "Subpicosecond electro-optic sampling: principles and applications", *IEEE J. Quantum Electron* QE-22:69, (1986).
53. D.R. Dykaar, T.Y. Hsiang, and G.A. Mourou, An Application of Picosecond Electro-optic Sampling to Superconducting Electronics, IEEE Trans. Magn., MAG-21:230 (1985).

54. D.R. Dyaar, T.Y. Hsiang, and G.A. Mourou, Development of a picosecond cryosampler in: "Picosecond Electronics and Optoelectronics," G.A. Mourou, D.M. Bloom, and C.-H. Lee, eds., Springer-Verlag Berlin, Heidelberg (1985) p.249.
55. G.A. Mourou and K.E. Meyer, Subpicosecond Electro-optic sampling using coplanar strip transmission lines, *Appl. Phys. Lett.* 45:492 (1984).
56. W. J. Gallagher et al, Subpicosecond optoelectronic study of resistive and superconductive transmission lines, *Appl. Phys. Lett.* 50-350 (1987); C.-C Chi et al, Subpicosecond optoelectronic study of superconducting transmission lines, *IEEE Trans. Magn.* - in print.
57. F.H. Bouderous, D. Pascal, S. Laval "A comparison of interdigital and straight structures for a photoconductive detector, *IEEE Trans. Electron Devices* ED-32, (4) 836-837 (1985).
58. G. A. Mourou and S. Williamson, *Appl. Phys. Lett.* 41, 44 (1982).
59. S. Williamson, G. Mourou, and J.C.M. Li, *Phys. Rev. Lett.* 52, 2364 (1984).
60. R.S. Becker, G.S. Higashi, and J.A. Golovchenko, *Phys. Rev. Lett.* 52, 307 (1984).
61. I.N. Duling III, T. Norris, T. Sizer, P. Bado, and G.A. Mourou, *J. Opt. Soc. Am. B* 2, 616 (1985)
62. G. Mourou and W. Knox, *Appl. Phys. Lett.* 36, 623 (1980).
63. G. Mourou, W. Knox, and S. Williamson, *Laser Focus* 18, 97 (1982).
64. W. Sibbett, H. Niu, and M.R. Baggs, *Rev. Sci. Instrum.* 53, 758 (1982).
65. K. Kinoshita, M. Ito, and Y. Suzuki, *Rev. Sci. Instrm.* 58, 932 (1987).
66. J. L. Wiza, *Nucl. Instrum. Methods* 162, 587 (1979).
67. H. E. Elsayed-Ali, T.B. Norris, M.A. Pessot, and G.A. Mourou, *Phys. Rev. Lett.* 58, 1212 (1987).
68. J. H. Bechtel, *J. Appl. Phys.* 46, 1585, (1975).
69. F. Claro and G.D. Mahan, *J. Appl. Phys.* 66, 4213 (1989).
70. M. Izutsu, Y. Yamane, and T. Sueta, *IEEE J. Quant. Electron* QE-13, 287 (1977).
71. K. Kubota, J. Noda, and O. Mikami, *IEEE J. Quant. Electron* QE-16, 754 (1980).
72. F. J. Leonberger, *Opt. Lett.* 5, 312 (1980).
73. C. M. Gee, G. D. Thurmond, and H. N. Yen, *Appl. Phys. Lett.* 43, 998 (1983).
74. P. Buchman, H. Kaufmann, H. Melchoir, and G. Guekos, *Appl. Phys. Lett.* 46, 462 (1985).
75. D. M. Materna, Case Western Reserve University, Department of Electrical Engineering and Applied Physics, M.S. Thesis (1986).
76. J.F. Whitaker, T.B. Norris, G. Mourou and T.Y. Hsiang, *IEEE Trans. Microwave Theory Tech* MTT-35, 41 (1987).
77. J. F. Whitaker, R. Sobolewski, D.R. Dykaar, T.Y. Hsiang, and G.A. Mourou, *IEEE Trans. Microwave Theory Tech.* MTT-36, 277 (1988).
78. See for instance, I.P. Kaminov, An Introduction to Electro-optic Devices, (Academic Press, New York, 1974), p.228.
79. See for instance, E. Yamashita, K. Atsuki, and T. Ueda, *IEEE Trans. Microwave Theory Tech.* MTT-27, 1036 (1979).
80. F.W. Smith, A.R. Calawa, C.L. Chen, M.J. Manfra, and L.J. Mahoney, *IEEE Electron Dev. Lett.* EDL-9, 7 (1988).
81. F.W. SMith, A.R. Calawa, C.L. Chen, L.J. Mahoney, M.J. Manfra, and J.C. Huang, in Proceedings IEEE/Cornell Conference on Advanced Concepts in High Speed Semiconductor Devices and Circuits. 1987 (IEEE, New York, 1987), p.229.
82. F.W. Smith, C.L. Chen. G.W. Turner, M.C. Finn, L.J. Mahoney, M.J. Manfra, and A.R. Calawa, in Technical Digest 1988 IEEE International Electron Devices Meeting, San Francisco, CA (IEEE, New York, 1988), p. 838.
83. F.W. Smith, B.-Y. Tsaur, and A.R. Calawa (unpublished).
84. D.H. Auston, in *Picosecond Optoelectronic Devices*, edited by C.H. Lee (Academic, Orlando, 1984), pp. 73-117.

85. D. Strickland and G. Mourou, *Opt. Commun.* 56, 219 (1985).
86. M. Pessot, J. Squier, P. Bado, G. Mourou, and D. Harter, *IEEE J. Quantum Electron.* QE-25, 61 (1989).
87. R.L. Fork, C.H. Brito Cruz, P.C. Becker, and C.V. Shank, *Opt. Lett.* 12, 483 (1987).
88. J.C. Walling, O.G. Peterson, H.P. Jenssen, R.C. Morris, and E.W. O'Dell, *IEEE J. Quantum Electron.* QE-16, 1302 (1980).
89. L.F. Mollenauer and J.C. White, eds, *Tuanble Lasers* (Springer-Verlag, New York, 1987) p. 352.
90. A.E. Siegman, *Lasers* (University Science, Mill Valley, Calif., 1986), p.282.
91. B. Zysset, W. Hodel, P. Beaud, and H.P. Weber, *Opt. Lett.* 11, 156 (1986).
92. A.S. Gouveia-Neto, A.S.L. Gomes, and J.R. Taylor, *Opt. Lett.* 12, 395 (1987).

Publications and Conference Presentations

- H.E. Elsayed-Ali, T.B. Norris, M.A. Pessot, G.A. Mourou, "Time-Resolved Observation of Electron-Phonon Relaxation in Copper," *Phys. Rev. Lett.* 58, 1212-1215 (March 1987).
- P. Bado, M. Bouvier, J.S. Coe, "Nd:YLF Mode-Locked Oscillator and Regenerative Amplifier," *Opt. Lett.* 12, 319-321 (May 1987).
- P. Bado, I.N. Duling III, T. Sizer II, T.B. Norris, G.A. Mourou, "Generation of White Light at 1 KHz," Ultrashort Pulse Spectroscopy and Applications (SPIE, Bellingham, WA, 1985), Vol. 533, pp. 59-62.
- D.R. Dykaar, F. Sobolewski, T.Y. Hsiang, G.A. Mourou, "Response of a Josephson Junction to a Stepped Voltage Pulse," IEEE Trans. Magn. MAG-23, 767-770 (March 1987).
- M. Pessot, P. Maine, G.A. Mourou, "1000 Times Expansion/Compression of Optical Pulses for Chirped Pulse Amplification," *Opt. Commun.* 62, 419-421 (June 1987).
- H.E. Elsayed-Ali and G.A. Mourou, "Phase Transitions in the Picosecond Time Domain," Interfaces, Superlattices, and Thin Films, edited by J.D. Dow, (Materials Research Society, Pittsburgh, PA 1987) 77, pp. 51-57.
- T. Jackson, J. Nees, R. Vallee, and G.A. Mourou, "Novel Method for Ultrahigh-Frequency Electro-Optic Time-Domain Reflectometry," *Electron. Lett.* 23, 1130-1131 (October 1987).
- T.Y. Hsiang, J.F. Whitaker, P. Sobolewski, D.R. Dykaar, and G.A. Mourou, "Propagation Characteristics of Picosecond-Electrical Transients on Coplanar Striplines," *Appl. Phys. Lett.* 51, 1551-1553 (November 1987).
- H.E. Elsayed-Ali and G.A. Mourou, "Picosecond Reflection High-Energy Electron Diffraction," *Appl. Phys. Lett.* 52, 103-104 (January 1988).
- D.R. Dykaar, R. Sobolewski, J.M. Chwalek, T.Y. Hsiang, and G.A. Mourou, "Electro-Optic Sampler for Characterization of Devices in a Cryogenic Environment," Advances in Cryogenic Engineering Vol 33, edited by R. W. Fast (Plenum Publishing corporation, 1988), pp. 1097-1104.
- J.F. Whitaker, R. Sobolewski, D.R. Dykaar, T.Y. Hsiang, and G.A. Mourou, "Subpicosecond Pulse Propagation on Superconducting Striplines," *Jpn. J. Appl. Phys.* 26, 1563-1564 (1987).
- J.F. Whitaker, R. Sobolewski, D.R. Dykaar, T.Y. Hsiang, and G.A. Mourou, "Propagation Model for Ultrafast Signals on Superconducting Dispersive Striplines," *IEEE Trans. Microwave Theory Tech.* 36, 277-285 (February 1988).
- G. Mourou, "High Speed Circuit Testing Using Ultrafast Optical Techniques," Microelectronic Engineering 7, 343-349 (1987).
- D.R. Dykaar, R. Sobolewski, J.M. Chwalek, J.F. Whitaker, T.Y. Hsiang, G.A. Mourou, D.K. Lathrop. S.E. Russek, and R.A. Buhrman, "High-Frequency Characterization of Thin-Film Y-Ba-Cu Oxide Superconducting Transmission Lines," *Appl. Phys. Lett.* 52, 1444-1446 (April 1988).

- G.A. Mourou, D. Dykaar, J. Chwalek, and J.F. Whitaker, "Superconducting Interconnects," Proceedings of SPIE Conference on Advances in Semiconductors and Superconductors: Physics and Device Applications, Newport Beach, California (March 1988).

- P. Bado, M. Pessot, J. Squier, G.A. Mourou, and D.J. Harter, "Regenerative Amplification in Alexandrite of Pulses from Specialized Oscillators," *IEEE J. Quantum Electron. 24*, 1167-1171 (June 1988).

- J.M. Chwalek, D.R. Dykaar, J.F. Whitaker, R. Sobolewski, S. Gupta, T.Y. Hsiang, and G.A. Mourou, "Ultrafast Response of Superconducting Transmission Lines," presented at Applied Superconductivity Conference, San Francisco, California (August 1988).

- J.F. Whitaker, G.A. Mourou, T.C.L.G. Sollner and W.D. Goodhue, "Picosecond Switching-time Measurement of a Resonant-tunneling Diode," *Appl. Phys. Lett.*, Vol. 53, pp. 385-387 (August 1988).

- K. Meyer, M. Pessot, and G.A. Mourou, "Subpicosecond Photoconductivity Overshoot in Gallium Arsenide Observed by Electro-Optic Sampling," *Appl. Phys. Letts.*, Vol. 53, pp. 2254-2256 (September 1988).

- K. Meyer, M. Pessot, and G. Mourou, "Subpicosecond Photoconductivity Overshoot in Gallium Arsenide Observed by Electro-Optic Sampling," *Appl. Phys. Lett.* 5, 2254-2256 (December 1988).

- D. R. Dykaar, R. Sobolewski, J. M. Chwalek, T. Y. Hsiang, and G. A. Mourou, "Electro-Optic Sampler for Characterization of Devices in a Cryogenic Environment," Advances in Cryogenic Engineering , edited by R. W. Fast (Plenum Publishing Corporation, 1988), Vol. 33, pp. 1097-1104.

- J. M. Chwalek, D. R. Dykaar, J. F. Whitaker, T. Y. Hsiang, G. Mourou, D. K. Lathrop, S. E. Russek, and R. A. Buhrman, "Picosecond Transient Propagation Studies on Thin-film Y-Ba-Cu-O Transmission Lines," Ultrafast Phenomena VI (Springer-Verlag, New York, 1988), p. 201.

- J. Nees, S. Williamson, and G. Mourou, "Greater than 100 GHz Traveling Wave Modulator," Ultrafast Phenomena VI, (Springer-Verlag, New York, 1988), p. 205.

- K. Meyer, M. Pessot, G. A. Mourou, R. Grondin, and S. Chamour, "Subpicosecond Photoconductivity Overshoot in GaAs Observed by Electo Optic Sampling," *Appl. Phys. Letts.* 53, pp. 2254 (1988).

- T.B. Norris, X.J. Song, W.J. Schaff, L.F. Eastman, G. Wicks, and G.A. Mourou, "Tunneling Escape Time of Electrons from a Quantum Well under the Influence of an Electric Field," *Appl. Phys. Lett.* 54, 60-62 (January 1989).

- M. Pessot, J. Squier, P. Bado, G. Mourou, D.J. Harter, "Chirped Pulse Amplification of 300fs Pulses in an Alexandrite Regenerative Amplifier," *IEEE J. Quantum Electron.* 25, 61-66 (January 1989).

- J. F. Whitaker, T. B. Norris, G. A. Mourou, T.C.L.G. Sollner, W. D. Goodhue, and X. J., "Switching times of resonant tunneling diodes," presented as an invited talk at the March Meeting of the American Physical Society, St. Louis, MO (March 1989).

- F. W. Smith, S. Gupta, H. A. Le, M. Frankel, V. Diadiuk, M. A. Holiis, D. R. Dykaar, G. A. Mourou, A. R. Calawa, "Picosecond GaAs-based photoconductive optoelectronic detectors", *Appl. Phys. Lett.* 54, 10, pp. 890 (March 1989).

- J. Nees, S. Williamson, and G. Mourou, "100 GHz Traveling-wave Electro-Optic Phase Modulator," *Appl. Phys. Lett.* 54, 1962-1964 (May 1989).

- T.B. Norris, N. Vodjdani, B. Vinter, C. Weisbuch, G.A. Mourou, "Charge-Transfer State Photoluminescence in Asymmetric Coupled Quantum Wells," accepted for publication in *Physical Review Letters*, 1 May 1989.

- M.Y. Frankel, S. Gupta, J.A. Valdmanis, and G.A. Mourou, "Picosecond Pulse Formation by Transmission Line Discontinuities," *Electronics Letters* 25, 20, (September 1989).

- J.F. Whitaker, J.A. Valdmanis, T.A. Jackson, K.B. Bhasin, R. Romanofsky, and G.A. Mourou, "External Electro-Optic Probing of Millimeter-Wave Integrated Circuits," *1989 IEEE MTT-S International Microwave Symposium Digest* 1, 221-224 (June 1989).

- J.M. Chwalek and D.R. Dykaar, "A Mixer Based Electro-Optic Sampling System for Submillivolt Signal Detection", submitted to *Review of Scientific Instruments*, July 1989.

- T.B. Norris, N. Vodjdani, B. Vinter, C. Weisbuch, and G.A. Mourou, "Charge-Transfer State Photoluminescence in Asymmetric Coupled Quantum Well," *Phys. Rev. B* 40, 1392-1395 (July 1989).

- T.B. Norris, X.J. Song, G. Wicks, W.J. Schaff, L.F. Eastman, and G.A. Mourou, "Electric Field Dependence of the Tunneling Escape Time of Electrons from a Quantum Well," Picosecond Electronics and Optoelectronics III, vol. 4, 121-123 (OSA, Washington, 1989).

- T.B. Norris, N. Vodjdani, B. Vinter, C. Weisbuch, and G.A. Mourou, "Time-Resolved Observation of Luminescence from a Charge-Transfer State in Double Quantum Wells," scheduled for publication in Quantum Wells for Optics and Optoelectronics, (OSA, Washington, 1989).

- F.W. Smith, S. Gupta, H.Q. Lee, M. Frankel, V. Diadiuk, M.A. Hollis, D. R. Dykaar, G.A. Mourou, A. R. Calawa, "Picosecond GaAs-based Photoconductive Optoelectronics Detectors," scheduled for publication in Picosecond Electronics and Optoelectronics III, edited by D. M. Bloom & T. C. L. G. Sollner (OSA, Washington, 1989).

- S.N. Chamoun, R. Joshi, A.N. Arnold, R. Grondin, K. Meyer, M. Pessot, and G.A. Mourou, "Theoretical and Experimental Investigations of Subpicosecond Photoconductivity," submitted to *Opt. Letts.*.

- F.W. Smith, S. Gupta, H.Q. Lee, M. Frankel, V. Diadiuk, M.A. Hollis, D.R. Dykaar, G.A. Mourou, A.R. Calawa, "Picosecond GaAs-Based Photoconductive Optoelectronics Detectors," *Appl. Phys. Lett.*, 54, pp. 890 (1989) .

- H-C. Chen, G.A. Mourou, and R. Knox, "Subnanosecond Time-Resolved Electron Diffraction from Thin Crystalline Gold Films," to be considered for publication in *Phys. Rev. Lett.*

- G. Vaillancourt, T.B. Norris, J.S. Coe, and G.A. Mourou, "Operation of a 1-kHz Pulse-pumped Ti:sapphire Regenerative Amplifier, " *Optics Letters*, 15, 317-319 (March 1990).

- J.M. Chwalek, C. Uher, J.F. Whitaker, and G.A. Mourou, J. Agostinelli and M. Lelental, "Femtosecond Optical Absorption Studies of Nonequilibrium Electronic Processes in High-T_C Superconductors," submitted to *Applied Physics Letters* (May 8, 1990).

- P. Bado, J.S. Coe, J. Squier, F. Salin, C.-Y. Chien, J.-L. Tapié, and G. A. Mourou, "Ultrahigh Peak Power Generation: Present & Future," submitted to Ultrafast Pheomena Meeting, Monterey, California, May 14-25, 1990.

Personnel and Awarded Degrees

This is the list of participants and scientists and graduate students involved in the URI project at the University of Rochester and Cornell.

University of Rochester

Faculty and Scientists

G. Mourou

D. Dykaar	Superconductivity, High-speed devices
T. Hsiang	Characterization, Transport in semiconductors
T. Jackson	Transport in semiconductors,
R.J. Knox	High-speed device characterization, Superconducting traveling-wave transistor
W. Donaldson	High-speed switching
H. El-Sayed Ali	Picosecond RHEED
S. Williamson	100-GHz optical modulator
J. Nees	High-speed electronic characterization
P. Bado	Ultrafast laser technique
M. Bouvier	Electronics support
S. Coe	Optics support

Graduate Students

M. Frankel	High-speed device characterization
S. Gupta	High-speed device characterization
J. Chwalek	Millimeter-wave properties of High-Tc superconductor
T. Norris	Tunneling in quantum wells
J. Whitaker	Response of resonant tunneling diode
D. Strickland	Amplification of ultrashort optical pulses
C. Hsiu-Cheng	Time-resolved electron diffraction
J. Squier	Amplification of ultrashort optical pulses
M. Pessot	Generation and amplification of ultrashort optical pulses

Ph.D. Degrees Awarded

University of Michigan

Hsiu-Chen Chen	1989	*Subnanosecond Time-Resolved Electron Diffraction Studies of Short-Pulse Laser Heating in Thin Gold Films.*
Theodore Norris	1989	*Time-Resolved Tunneling in GaAs Quantum Well Structures*
Maurice Pessot	1989	*Chirped Pulse Amplification of Femtosecond Optical Pulses*
Donna Strickland	1988	*Amplification of Ultrashort Pulses with Chirped Pulse Amplification*
Kevin Meyer	1988	*Study of Subpicosecond Electron Transport in GaAs*
John Whitaker	1988	*Ultrafast Optics for the Study of the Propagation of Ultrashort Electrical Pulses and the Response of Resonant Tunneling Diode.*
Doug Dykaar	1987	*Picosecond Switching Measurements of a Josephson Tunnel Junction*

Cornell University

Xiao Song	1990
Doug Shire	1989

Knowledge Transfer

A. Interaction with Outside Laboratories

During the URI contract five industrial, two government and four university laboratories have sent 18 researchers to share our facility. More than 15 refeered publications have subsequently been produced.

The list of these institutions appears below:

Laboratories	Investigations	Projects
University of Illinois	Higman, Coleman	Heterostructure Hot Electron Diodes
NASA Lewis Res. Center	K. Bhasin	Monlithic Microwave Transistor Circuits
General Electric	G. Duh	High-electron Mobility Transistor
MIT Lincoln Lab	Sollner, Goodhue	Resonant Tunneling Diode
	Callawa	Low-Temperature MDE Grown GaAs
	Murphy	Permeable Base Transistor
Cornell University	Bhurman	High-Tc Superconductor
	Eastman	Travelling Wave Transistor
University of Rochester	Hsiang	Josephson Junctions, Devices
	Kadin	High Tc Superconductor
Bell Northern	P. Jay	FETs
Fujitsu	O. Wada	Photodiode
Arizona State University	B. Grondin	Velocity Overshoot
		Monte Carlo Simulation
Scientific Research Assoc.	M. Osman	Nonstationary Transport
	H. Grubin	Monte Carlo Simulation
Thomson-CSF	C. Weisbuch	Nonstationary Transport
Siemens	G. Solkner	Circuit Testing

B. Workshops

250 East River Road
Rochester New York 14623

Laboratory for Laser Energetics UR LLE

TEL 716 275 5101

TECHNICAL PROGRAM

URI REVIEW

November 5 - 6, 1987
(Coliseum)

Thursday, November 5th, Afternoon

2:30 PM	Welcome	Dean B. Arden Univ. of Rochester
2:40	Rochester Program an Overview	G. Mourou Univ. of Rochester
3:00	General Overview and Summary of Interaction	L.F. Eastman Cornell University
3:20	Theory of Transport Between Quantum Wells	R.S. Knox Univ. of Rochester
3:50	**BREAK**	
4:10	Switching Mechanisms in Heterostructure Hot Electron Diode	J.J. Coleman Univ. of Illinois
4:20	Transport Between Quantum Wells (Experiments)	T. Norris Univ. of Rochester
4:35	Tunneling Time Measurement by Photoluminescence	J. Song Cornell University
4:45	The Resonant Tunneling Diode	R.A. Murphy MIT Lincoln Lab
4:55	Switching Time of Resonant Tunneling Diode (Theory)	D. Coon Univ. of Pittsburgh
5:05	Switching Time of Resonant Tunneling Diode (Experiment)	J. Whitaker Univ. of Rochester
5:15	Investigation by Raman Spectroscopy of the Effect of Growth Stops at GaAs/GaAlAs	J.T. Bradshaw Cornell University

250 East River Road
Rochester, New York 14623

Laboratory for Laser Energetics UR LLE

TEL 716 275 5101

TECHNICAL PROGRAM
URI REVIEW

November 5 - 6, 1987
(Coliseum)

Continued

Friday, November 6, Morning

8:30 AM	Velocity Overshoot Monte Carlo Simulation	R. Grondin Arizona State Univ.
8:45	Velocity Overshoot Experimental Study	K. Meyer Univ. of Rochester
9:00	Electron Phonon Interaction A Picosecond Study	H. Elsayed-Ali Univ. of Rochester
9:20	Traveling Wave HEMT	D. Shire (Cornell Univ.) T. Jackson (Univ of Roch)
9:35	High Temperature Superconductors	R. Buhrman Cornell University
9:50	Propagation of Picosecond Electrical Pulses on Superconducting Lines	J. Chwalek Univ. of Rochester
10:05	**BREAK**	
10:20	Device and Test Interactions	P. Tasker Cornell University
10:35	High Speed Device Characterization	D. Dykaar Univ. of Rochester
10:50	MMIC Characterization	J. Nees, J. Whitaker Univ. of Rochester
11:05	Electro-optic Network Analyzer	T. Jackson Univ. of Rochester
11:20	MODFET Operation Beyond the Charge Control Model	L.D. Nguyen Cornell University
11:35	Closing Remarks	G. Mourou, Rochester L. Eastman, Cornell G. Witt, AFOSR

250 East River Road
Rochester, New York 14623

Laboratory for Laser Energetics
UR
LLE

TEL 716 275 5101

ROCHESTER-CORNELL WORKSHOP

on

Ultrafast Optics for Physics of Microstructures and High Speed Electronics

(2 September 1988)

9:00 AM	Introductory Remarks	G. Mourou - Rochester L. Eastman - Cornell
9:10	The Traveling Wave Transistor	D. Shire - Cornell T. Jackson - Rochester
9:30	Time-Resolved Tunneling in Quantum Well Structures	X. Song - Cornell T. Norris - Rochester
9:50	Direct Measurement of Resonant Tunneling Time	J. Whitaker - Rochester
10:10	Velocity Overshoot	R. Grondin - Arizona State Univ.
10:30	Coffee	
10:50	Single Picosecond Pulse Generation with Low Temperature Grown MBE Photoconductive Switches	F. Smith - MIT Lincoln Lab S. Gupta - Rochester
11:10	A New Ultrafast fs. Spectroscopic Source	M. Pessot - Rochester
11:30	> 100 GHz Optical Modulator	J. Nees - Rochester
12:00 PM	Lunch	

250 East River Road
Rochester, New York 14623

Laboratory for Laser Energetics UR LLE

TEL 716 275 5101

ROCHESTER-CORNELL WORKSHOP

on

Ultrafast Optics for Physics of Microstructures and High Speed Electronics

(2 September 1988)

Continued -

1:00 PM	Electro-Optic Probing of Digital Circuits	J. Valdmanis - ATT-Bell Lab
1:30	MBE Advances in 1987/88	B. Schaff - Cornell
1:45	High Speed Transistor Advances in 1987/88	P. Tasker - Cornell
2:00	High Speed Vertical Transistor	K. Yamasaki - NTT Corp.
2:15	Modeling of MODFET Transistors	M. Foisy - Cornell
2:30	Pseudomorphic AlGaAs/InGaAs MODFETS	L. Nguyen - Cornell
2:45	Pseudomorphic AlGaAs/InGaAs MODFET: and Characterization with Electro-Optic Technique	M. Frankel - Rochester
3:05	Coffee	
3:20	Al InAs/GaInAs MODFET on InP	L. Palmateer - Cornell
3:35	Self-Aligned Millimeter Wave HBT	D. Barker - Cornell
3:50	Propagation of Short Electrical Pulses on Superconducting Transmission Lines	J. Chwalek - Rochester

Cornell-Michigan-Rochester Workshop
on
Ultrafast Optics and High Speed Electronics
May 4, 1989
1311 EECS Building 8:30 - 5:00

8:30 Gerard Mourou, University of Michigan
Program Overview.

8:45 Lester Eastman, Cornell University
Program Overview.

9:05 Wayne Knox, AT&T Bell Labs
Exciton Dynamics in Heterostructures.

9:35 Theodore Norris, University of Michigan
Time-Resolved Tunneling in Quantum Wells.

9:55 BREAK

10:15 John Whitaker, University of Michigan
Time-Resolved Resonant Tunneling.

10:35 Duncan Steel, University of Michigan
Non-linear Spectrocopy of Resonant Tunneling Structures.

10:55 Jasprit Singh, University of Michigan
Transport in Lattice-Mismatched Epilayers.

11:15 R. Grondin, Arizona State University
Study of Velocity Overshoot through Time-Resolved Photoconductivity.

11:35 Hani Elsayed-Ali, University of Rochester
Hot-Electron Relaxation in Metals and Dynamics of Surface Melting.

12:05 LUNCH

1:30 Y.K. Chen, AT&T Bell Labs
High-Speed Heterostructures Bipolar Transistors.

2:00 George Duh, General Electric Company
High-Performance InP Lattice-Matched HEMT.

2:30 Todd Jackson, University of Rochester
Doug Shire, Cornell University
Superconductor Traveling-Wave MODFET.

2:50 Stephen Offsey, University of Cornell
Strained-Layer InGaAs-GaAs-AlGaAs Graded-Index, Separate Confinement Heterostructure, Single-Quantum-Well Laser Grown by MBE.

3:10 BREAK

3:30 Jánis Valdmanis, University of Michigan
Electro-Optic Sampling External vs. Internal Probing.

3:50 Shantanu Guptu, University of Michigan
Suspicosecond Electrical Pulses from Low-Temperature MBE-Grown GaAs.

4:05 Michael Frankel & Robert Voelker, University of Michigan
Picosecond Electrical Pulse Generation from Transmission Line Discontinuities.

4:30 WRAP UP

URI-AFOSR RESEARCH PROGRAM REVIEW

TRANSPORT IN MICROSTRUCTURES IN THE MICROWAVE & MM WAVE REGIME

Ultrafast Science Laboratory
The University of Michigan
Ann Arbor, Michigan 48109-2122

Friday, June 1, 1990

8:30-8:50	*Program overview* G. Mourou
8:50-9:10	*Role of transport in electronic and photonic devices* L. Eastman
9:10-9:40	*Time-resolved optical study of transport* T. Norris
9:40-10:00	*Hole-tunneling* J. Singh
10:00-10:15	*Coffee Break*
10:15-10:45	*Time-resolved electrical study of transport* J. Whitaker
10:45-11:05	*Novel resonant tunneling structure* X. Song
11:05-11:30	*Electro-optic network analysis* Mike Frankel
11:30-12:00	*Ultrashort pulses for time-resolved studies* J. Valdmanis
12:00-12:20	*Movie: "Light in Flight", directed and presented by* J. Valdmanis
12:20-2:00	*Lunch, Lab Tour and Posters*
2:00-2:20	*Multi hundred-GHz light modulators* S. Williamson
2:20-2:35	*60-GHz photoreceivers* K. Litvin
2:35-3:00	*Strained quantum well lasers for high speed - high frequency modulation* W. Shaff

3:00-3:20	*High resolution non-linear spectroscopy of resonant tunneling structures* D. Steel
3:20-3:40	*Raman study of sequential resonant tunneling* R. Merlin
3:40-4:00	*Coffee Break*
4:00-4:25	*Transport in high-T_c superconductors* J. Chwalek
4:25-4:50	*Transport in low-temperature-grown epitaxial semiconductors* Shantanu Gupta
4:50-5:00	*Closing remarks* G. Mourou, G. Witt

Figures

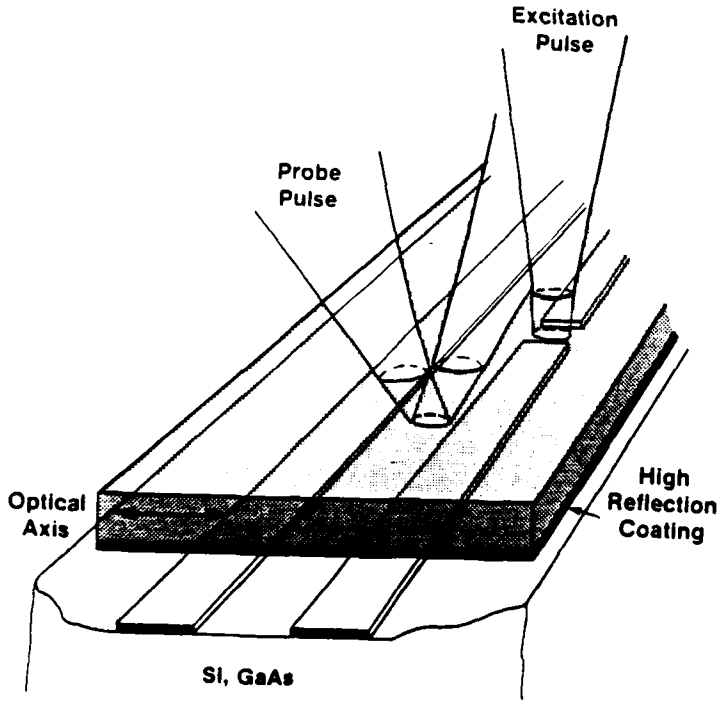

Fig. 1 Reflection-mode electro-optic sampling geometry.

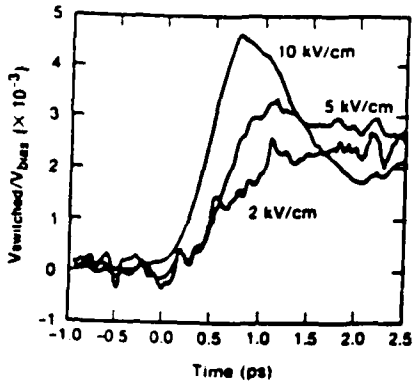

Fig. 2 Transient photoconductivity results for λ_{ex} = 620 nm. The plotted waveform is the transient voltage waveform generated by the photoconductive switch normalized to the applied dc voltage.

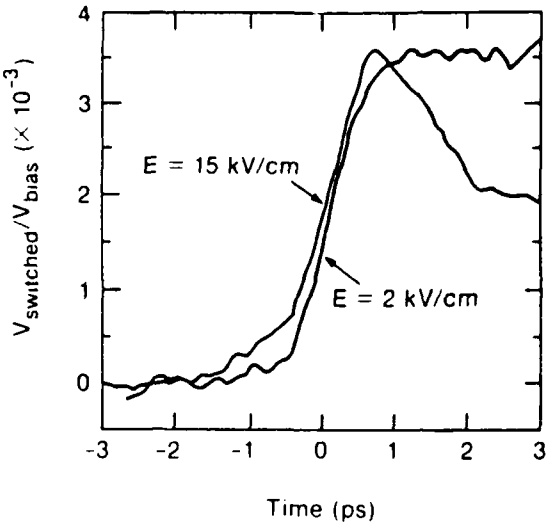

Fig. 3 Transient photoconductivity results of $\lambda_{ex} = 760$ nm

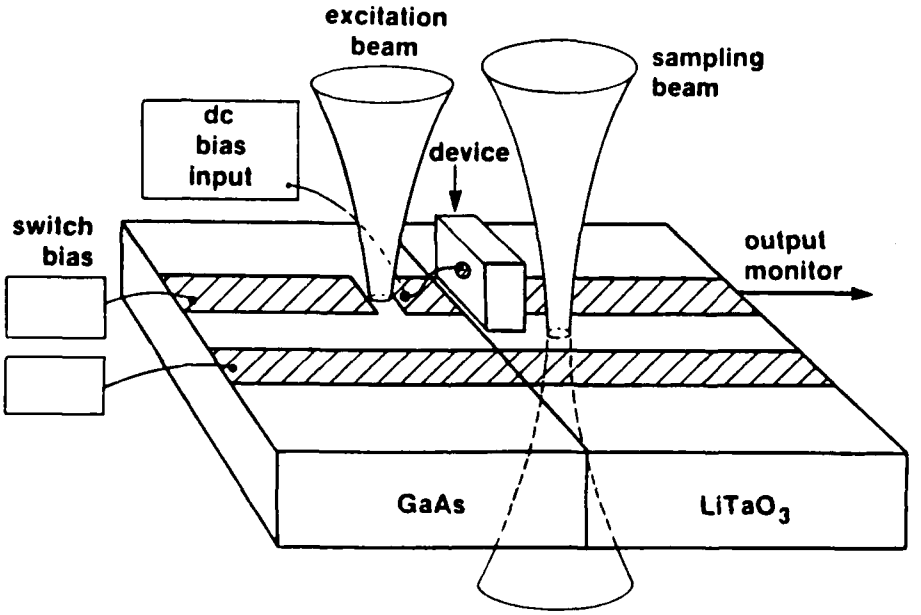

Fig. 4 Experimental configuration for electro-optic sampling of resonant-tunneling diode. A 12-μm-diam wire with a 1 μm tip contacts a mesa on the resonant-tunneling diode chip.

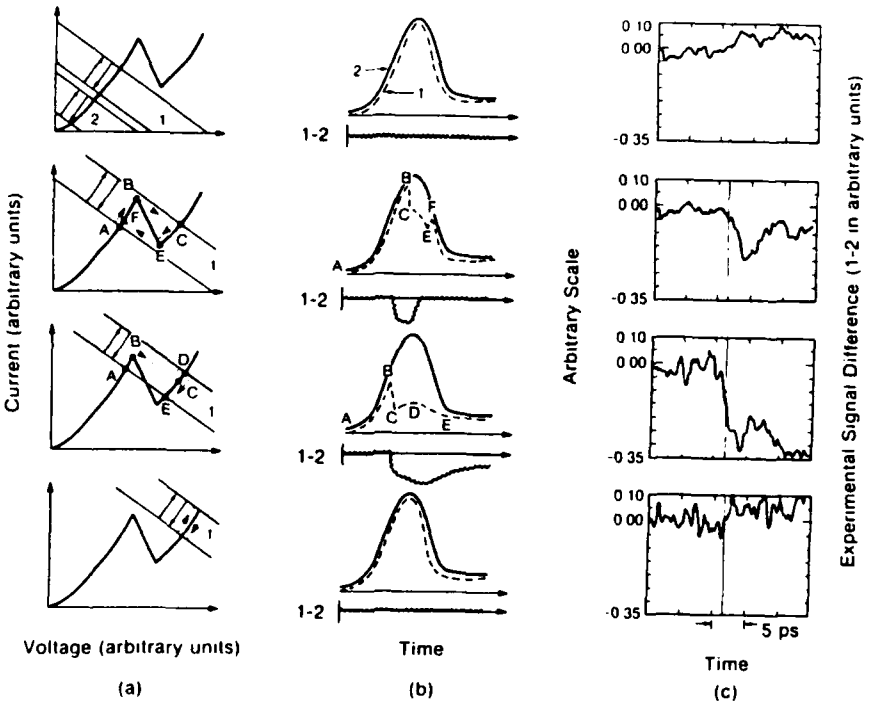

Fig. 5 Resonant-tunneling diode switching as a function of bias: (a) I-V curve with load lines, (b) analytic representation of waveforms resulting from movement of load lines in (a) and the difference of these waveforms, and (c) experimental signal difference.

p^+	$Al_xGa_{1-x}As$	2000 Å
i	$Al_xGa_{1-x}As$	2000 Å
i	GaAs	30 Å
i	$Al_xGa_{1-x}As$	b
i	GaAs	1000 Å
n^+	GaAs	1 μm

S I Substrate

Fig. 6 Structure of the single QW samples used in this study. The barrier width b was varied to study the effect on the tunneling rate.

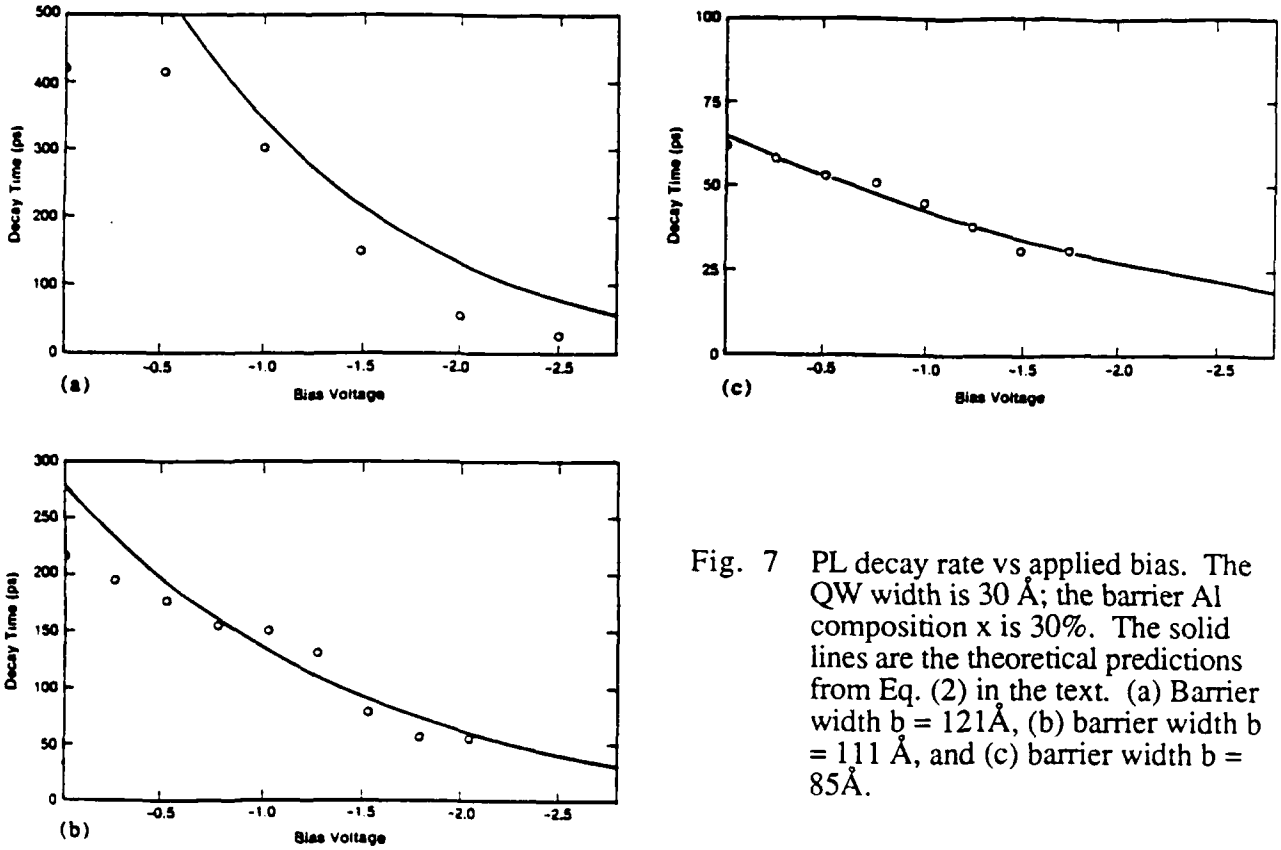

Fig. 7 PL decay rate vs applied bias. The QW width is 30 Å; the barrier Al composition x is 30%. The solid lines are the theoretical predictions from Eq. (2) in the text. (a) Barrier width b = 121Å, (b) barrier width b = 111 Å, and (c) barrier width b = 85Å.

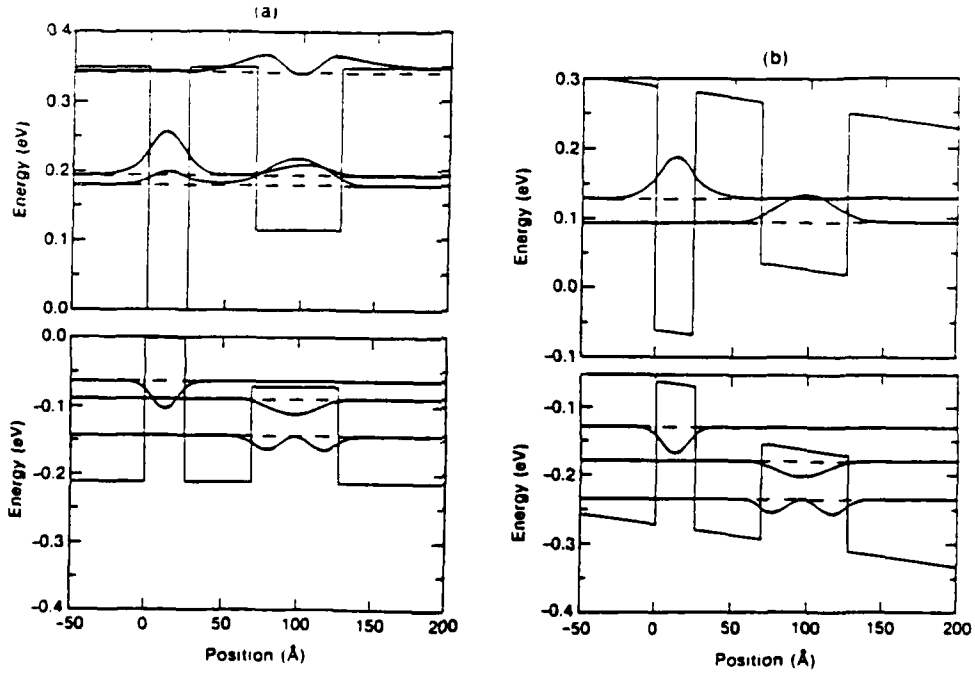

Fig. 8 Calculated band diagrams and electron and heavy-hole wave functions for sample A: (a) under flat-band conditions and (b) with an electric field of 30 kV/cm. The results for sample B are similar, but the electron states are always strongly localized in each well.

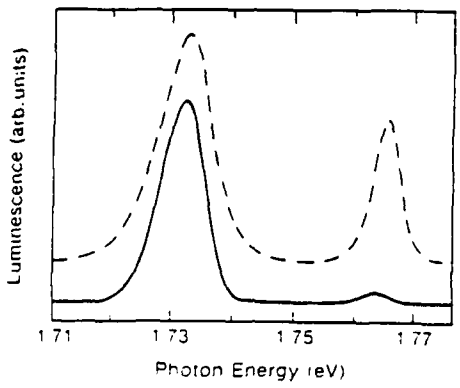

Fig. 9 Time-integrated PL spectra for sample A (solid line) and sample B (dashed line), with no applied bias voltage. The high-energy peak to QW2.

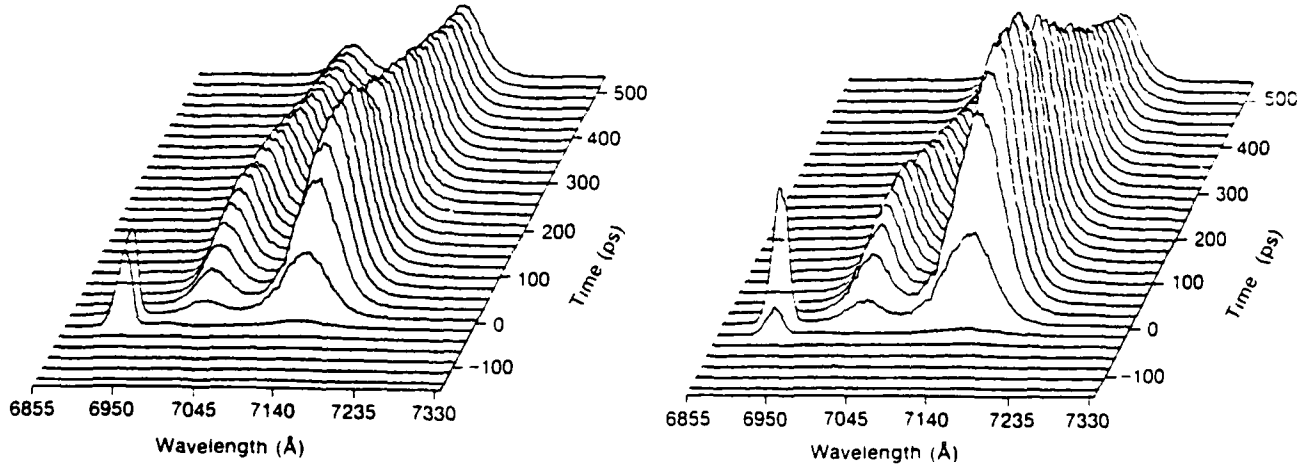

Fig. 10 Time-resolved PL spectra for sample B: (a) with no applied bias and (b) with -8V applied bias.

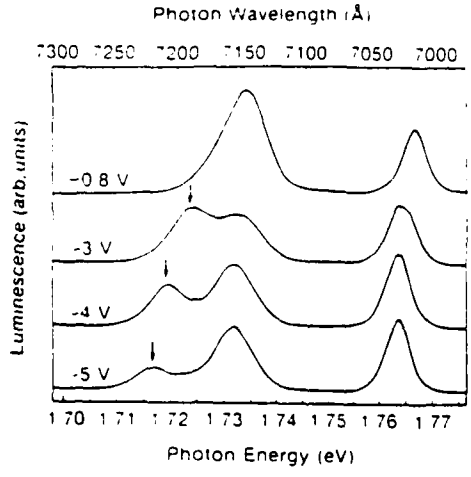

Fig. 11 Time-integrated PL spectra for sample B at various bias voltages.

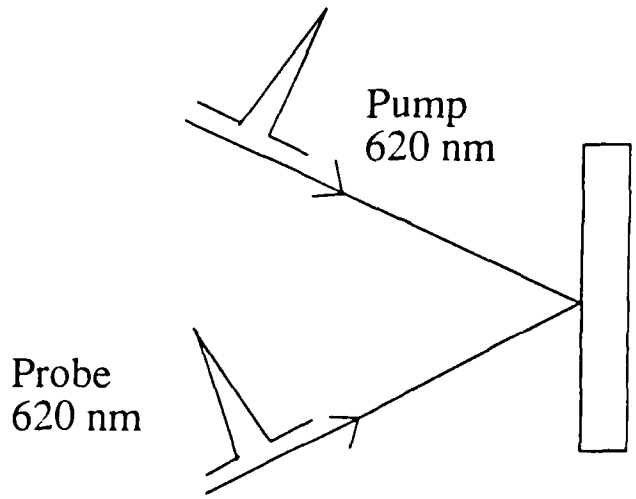

Fig. 12 Experimental setup to study the electron-phonon relaxation in metal.

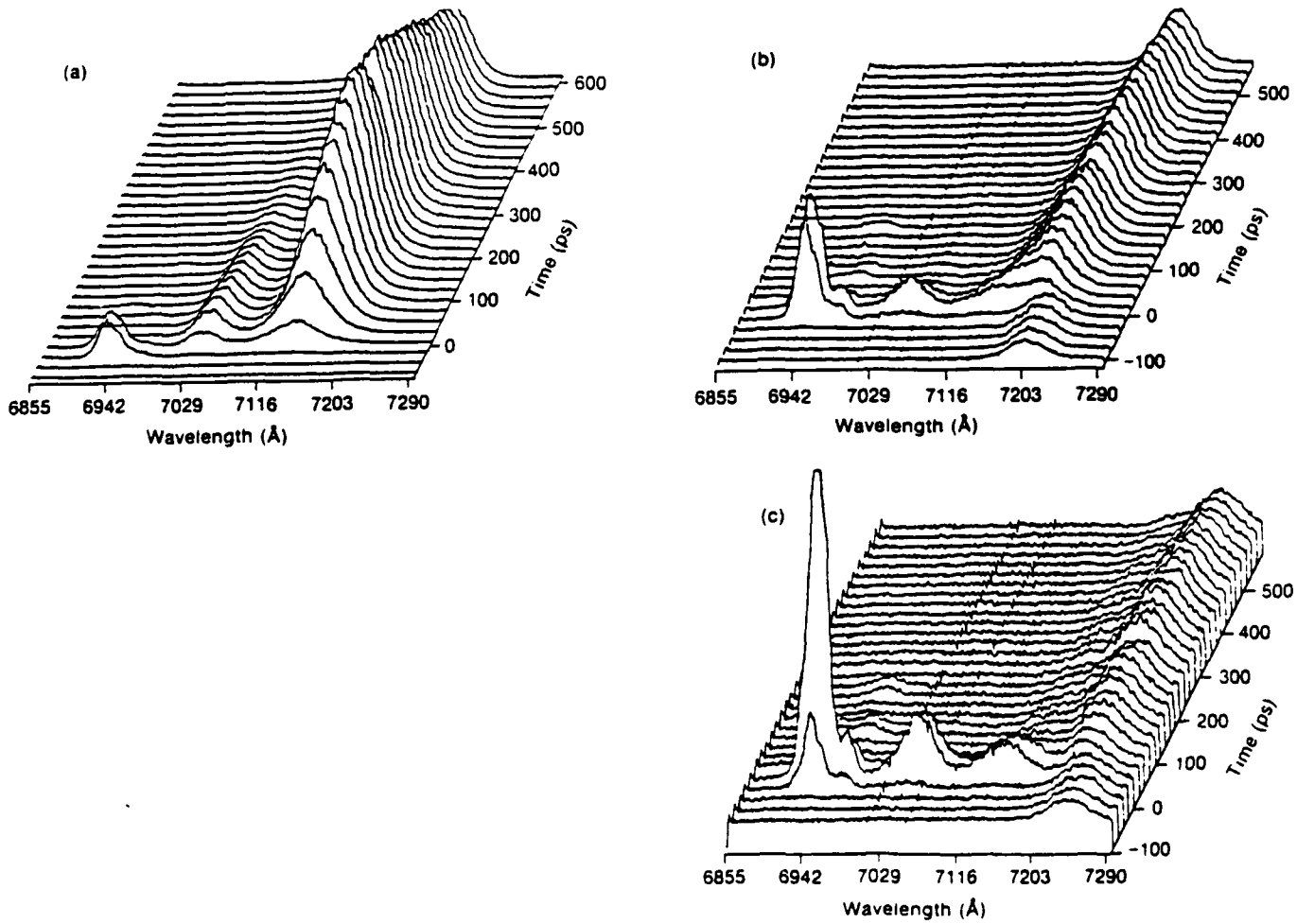

Fig. 13 Time-resolved PL spectra for sample A: (a) with o V, (b) -3V, and (c) -4.75 V applied bias.

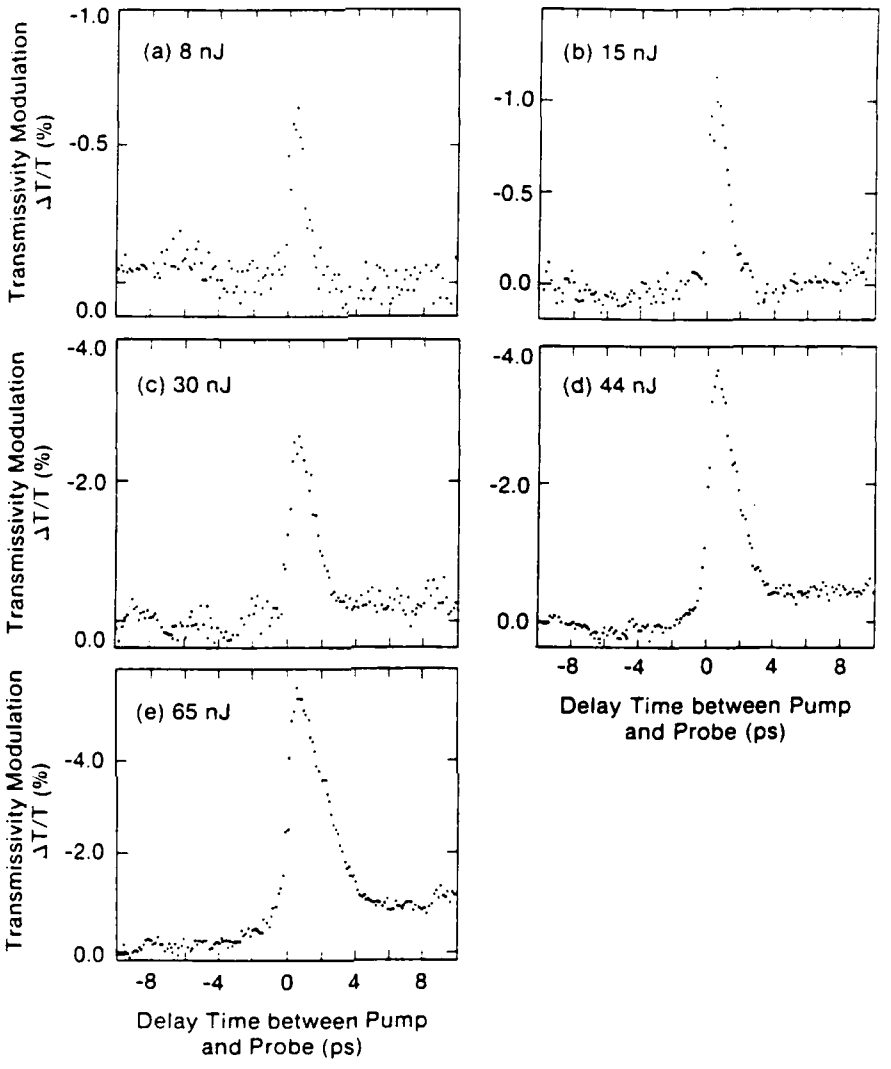

Fig. 14 Time-resolved transmissivity of ~200-Å Cu film at λ 620nm during laser heating (~300 fs FWHM) for different laser-pulse energies: (a) 8, (b) 15, (c) 30, (d) 44, and (e) 65 nJ. The heating laser was focused to ~27 μm; the probe laser to ~14μm and positioned near the center of the heating-laser spot.

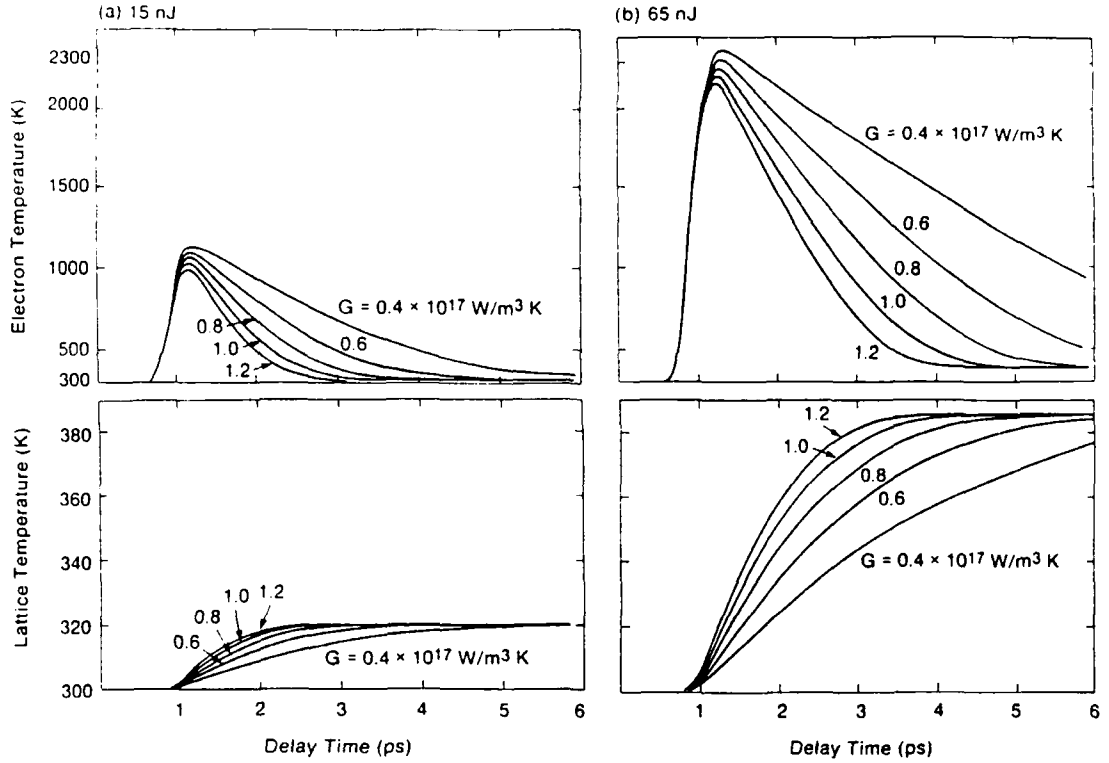

Fig. 15 Numerical modeling of the time evolution of electron and lattice temperatures for the experimental conditions in Figs. 14(b) and 14(e) [laser-pulse energy is (a) 15nJ and (b) 65nJ, with its peak at time = 1 ps]. Simulations were conducted for different values of the coefficient of heat transfer between the electrons and the lattice, G.

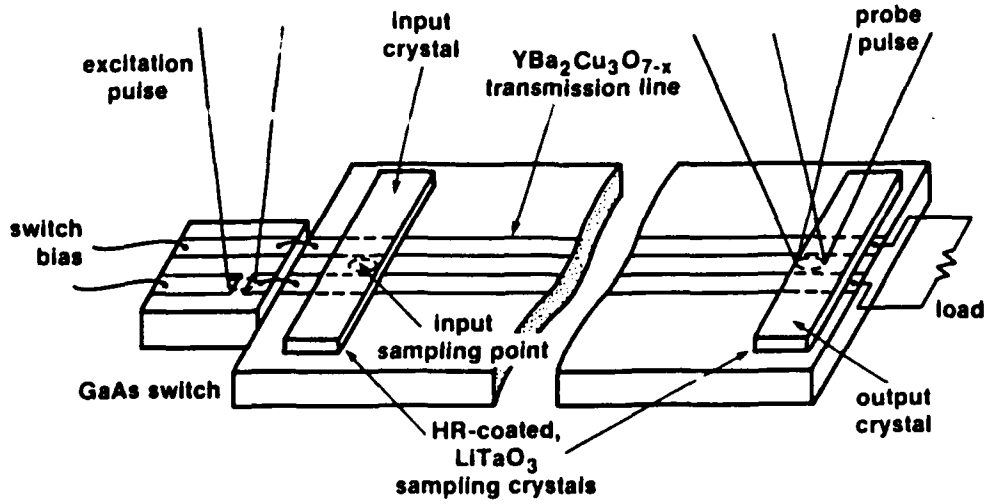

Fig. 16 Configuration of the samples used in this work.

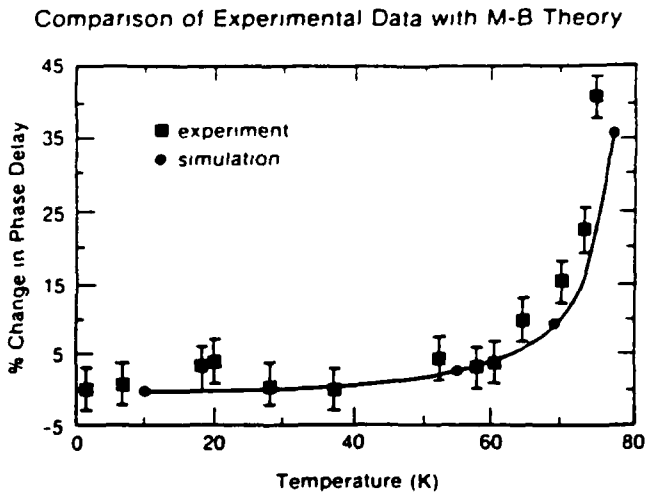

Fig. 17 Experimentally measured picosecond electrical transient propagation on the coplanar YBCO transmission line (sample 1). The small deviation at the very end of the output transient is probably due to a reflection from the sampling crystal.

Fig. 18 Measured waveforms from sample 2 (15 μm lines and spacing). The left-hand waveforms on the right show the transient response at the output sampling point as a function of temperature. Note that the delays are absolute: the time scale is calibrated while the amplitudes have been normalized to the input pulse.

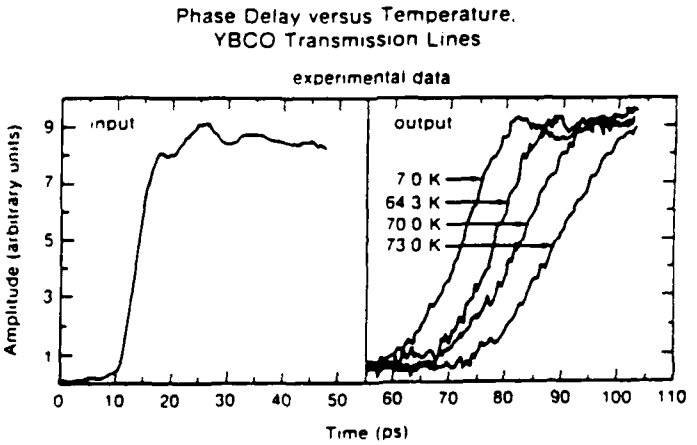

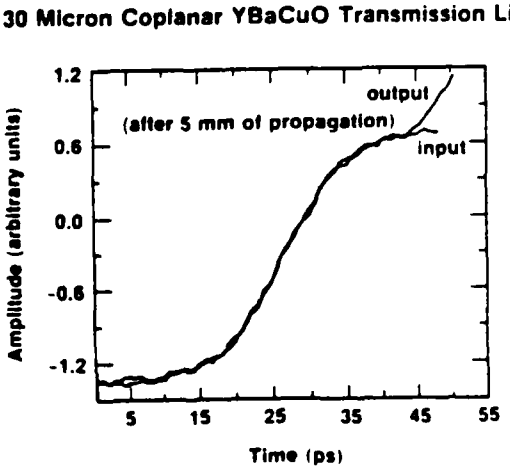

Fig. 19 Relative phase delays for the simulated (using Mattis-Bardeen complex conductivities) measured waveforms.

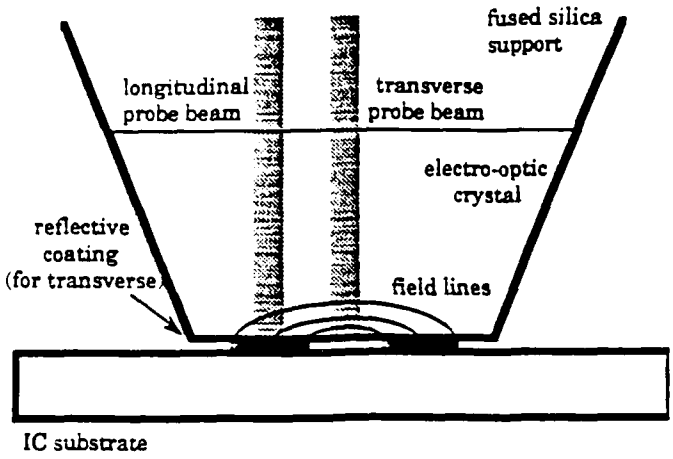

Fig. 20 (a) The external electro-optic probe tip, showing two different modulator configurations, transverse and longitudinal. With a transverse electro-optic crystal, the optical beam direction is perpendicular to the electric field lines fringing above an integrated circuit. With a longitudinal crystal, the optical beam and electric field lines are parallel. The probe beams represent a train of short laser pulses used to time-resolve an electrical signal.

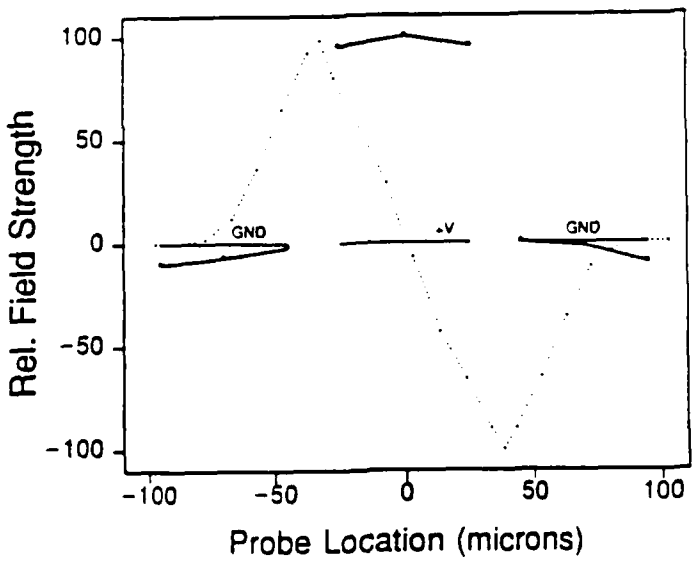

Fig. 20 (b) Field strength-which may be translated to voltage - as measured versus position on a a coplanar waveguide using external electro-optic sampling. The solid line indicates the field strength measured with the longitudinal KD*P crystal, while the dotted line indicates that measured using the transverse lithium tantalate crystal.

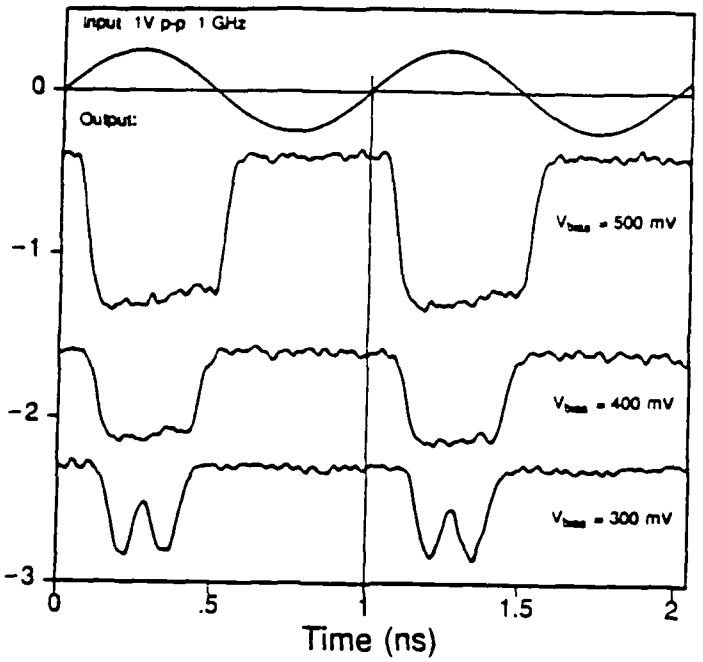

Fig. 21 Output of the inverting input buffer of a GaAs selectively doped heterostructure transistor (SDHT) prescaler integrated circuit with a 1-GHz input signal.

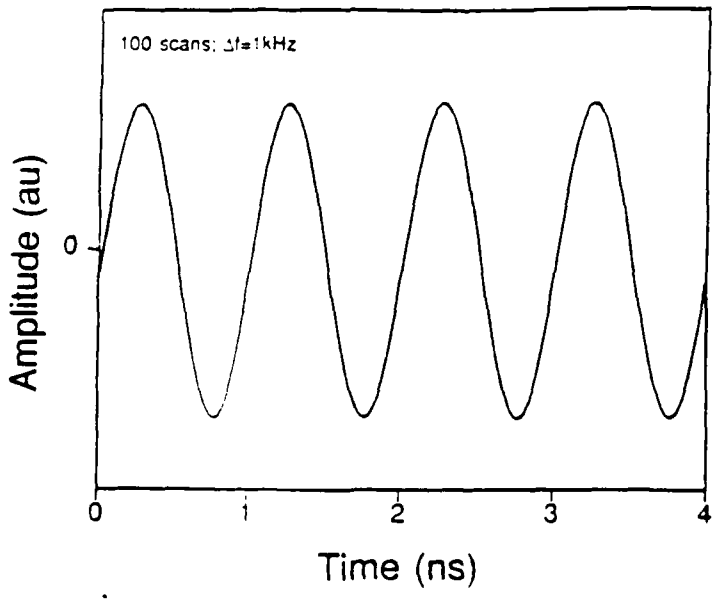

Fig. 22 1-GHz on-chip clock signal on a silicon 12-bit multiplexer integrated circuit.

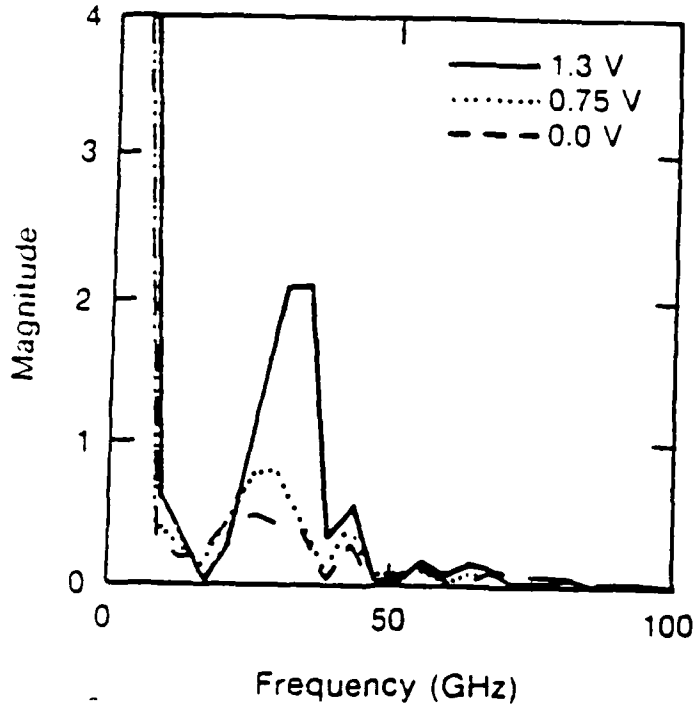

Fig. 23 Spectra of waveforms sampled at the output of a narrow-band MESFET single-stage amplifier MMIC for three different values of drain bias (up to saturation).

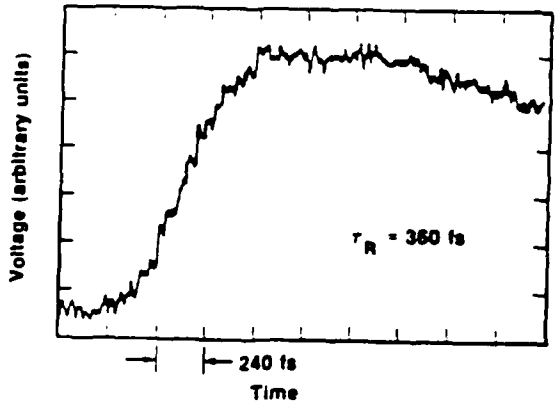

Fig. 24 Output waveform from the fully integrated cryogenic sampler. Rise time is about 360 fs.

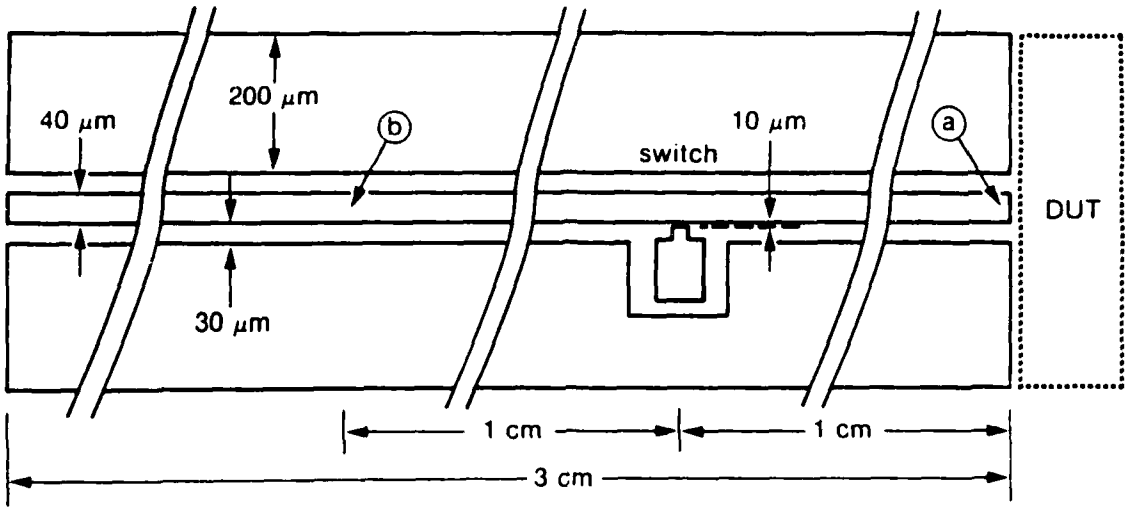

Fig. 25 Time-Domain Reflectometer Structure - A photoconductive switch is used in a coplanar waveguide to produce two identical counter propagating electrical pulses. One pulse travels towards the DUT, where as the other goes in opposite direction where it will be measured at a propagation distance equal to the distance between the switch and the DUT. This allows the independant characterization of the input and reflected pulse from DUT.

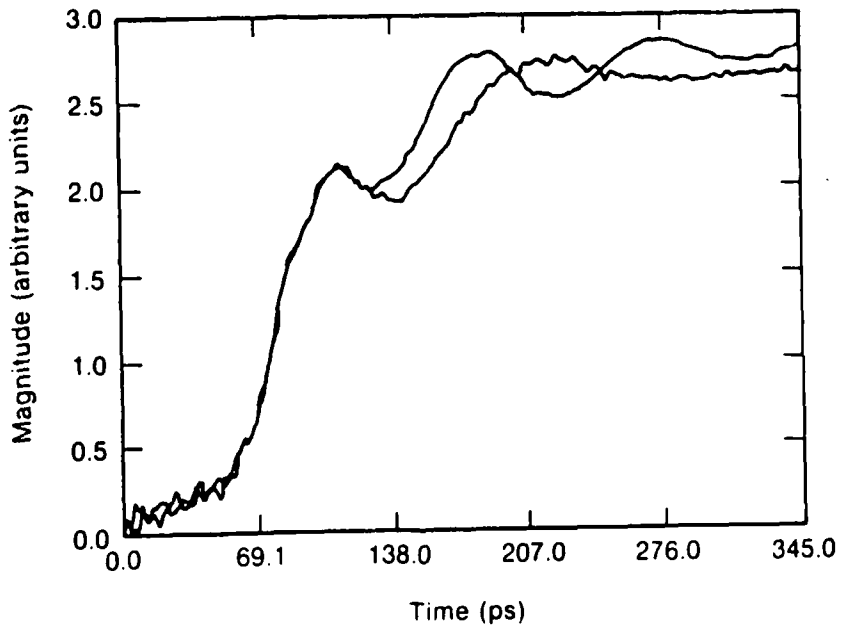

Fig. 26 Waveforms measured at two symetrical points with respect to the photoconductive switch. Notice that the two rising edges are identical.

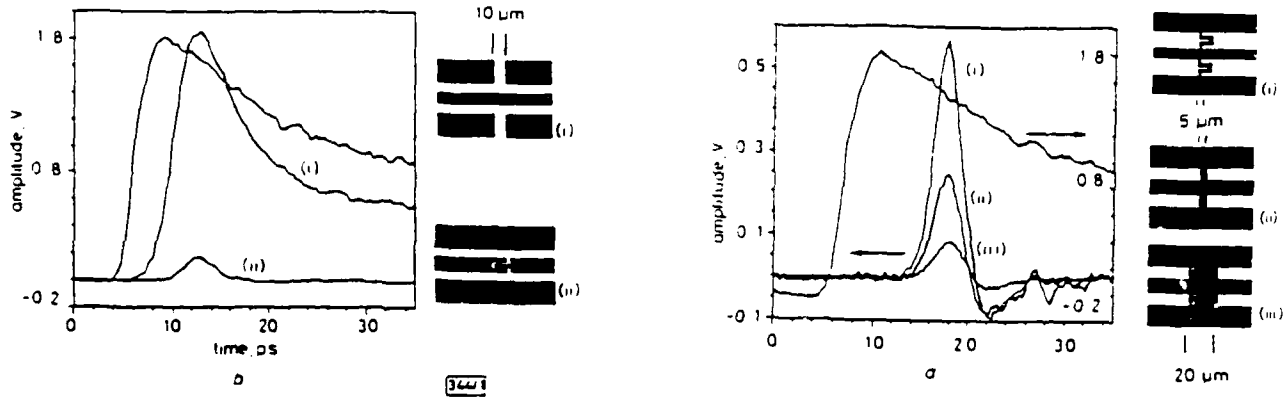

Fig. 27 (a) Step-like excitation and inductive shunt element outputs with corresponding discontinuity geometries (b) Step-like excitation and capacitive discontinuity outputs with corresponding geometry details. Amplitudes are accurate to ±15%

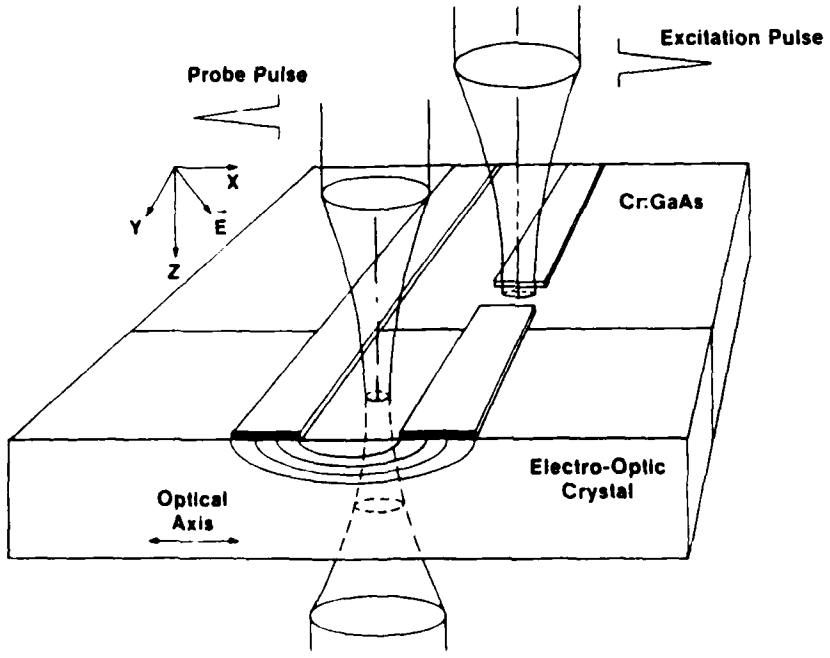

Fig. 28 Experimental configuration

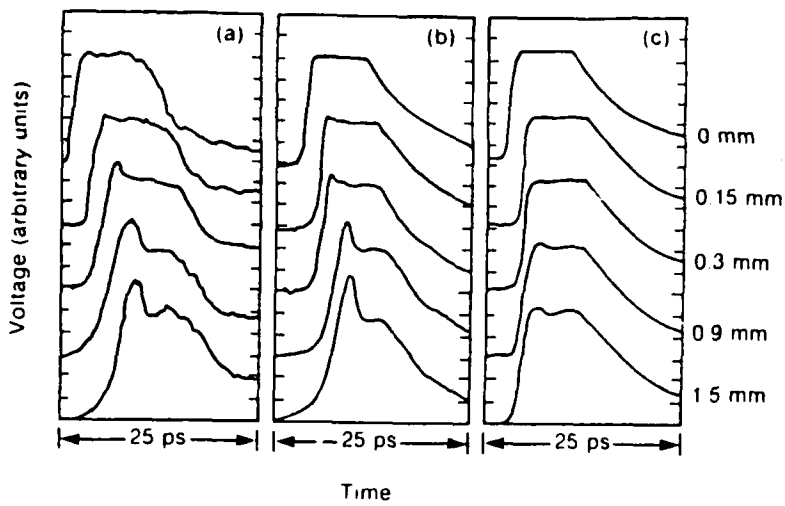

Fig. 29 Sequence of electrical transients propagated on the indium stripline in the superconducting state [T = 1.8K, critical temperature T_c = 3.4 K, energy gap Δ (0) ≈ 0.525 meV and $2\Delta/h$≈230 GHz, and resistivity at 4.2 K $\rho_{normal} \approx 2.7 \times 10^{-6}\ \Omega$ cm]. (a) Experimental results; (b) model computations with both the modal dispersion and Mattic-Bardeen effects taken into account; (c) model computations with modal dispersion neglected.

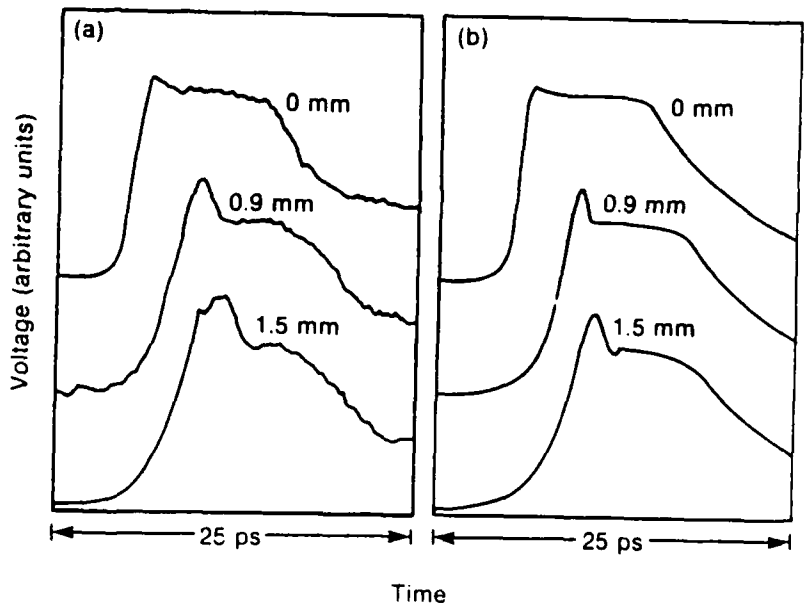

Fig. 30 Sequence of electrical transients propagated on the indium stripline in the normal state (T ≈ 6K). (a) Experimental results; (b) model computations.

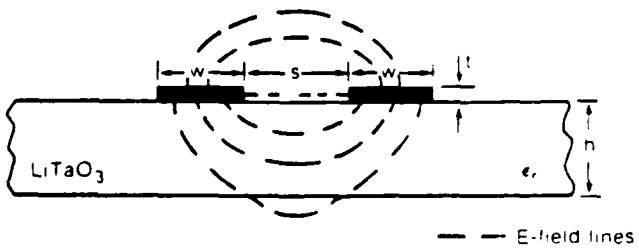

Fig. 31 Transverse cross section of the coplanar stripline with representative electric field lines shown.

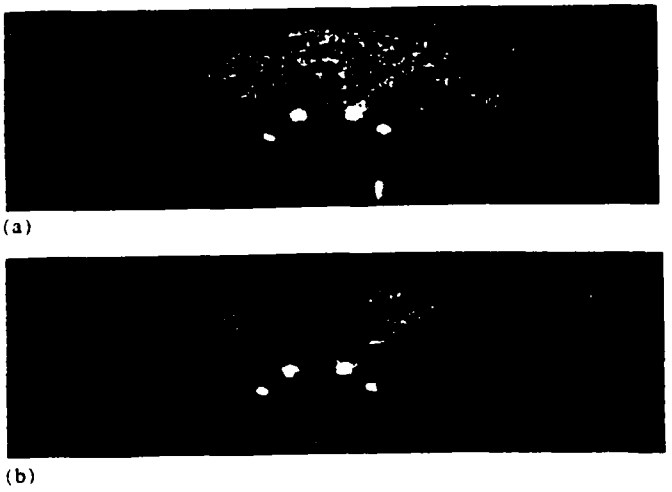

Fig. 32 Reflection high-energy electron diffraction patterns from a cleaved surface of a sodium chloride crystal: (a) using a single ~200-ps electron pulse; (b) after averaging 50 pulses. The microchannel plate gain was reduced for (b).

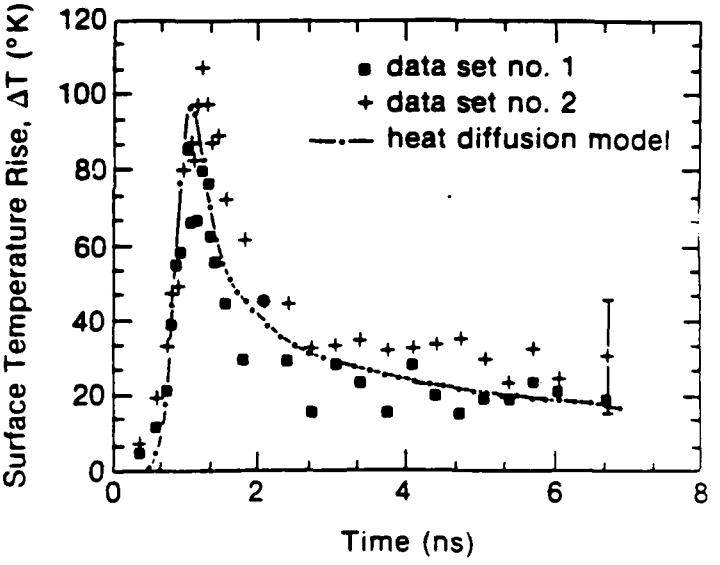

Fig. 33 Transient surface temperature rise of Pb(11) irradiated with 3.2 x 10^{u} W/cm^2 peak intensity, 350 ps FWHM, Nd:YAG (l = 1.06μm) laser pulses. Data sets 1 and 2 were obtained from the transient surface Debye-Waller effect on RHEED intensity using a static heating calibration. The solid line was obtained from a numerical heat diffusion model.

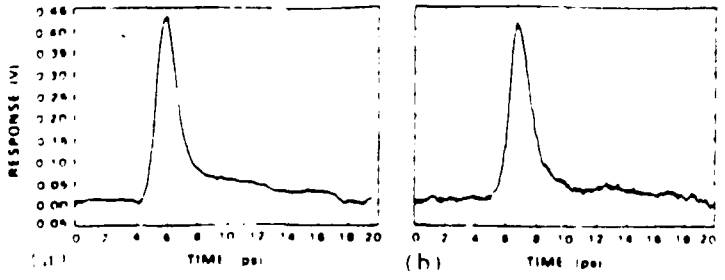

Fig. 34 Electrical impulse generated by a 70 fs laser pulse as measured by electro-optic sampling: (a) measured at point A and (b) measured at point B

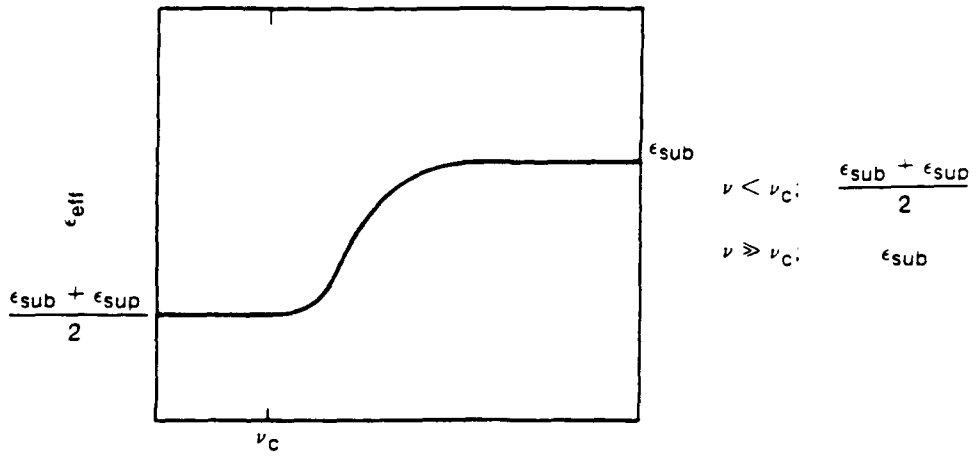

Fig. 35 Electrical dispersion due to dielectric mismatch.

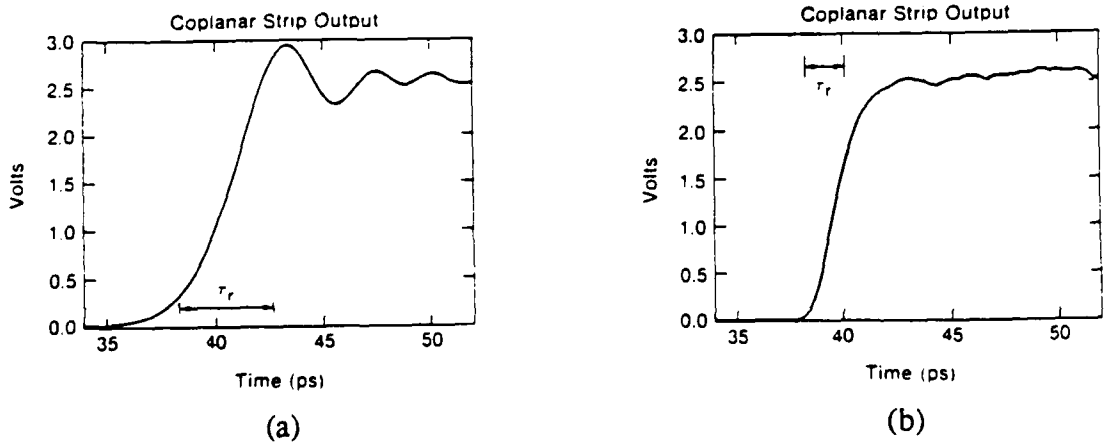

Fig. 36 Simulated propagation of signals with and without dielectric mismatch

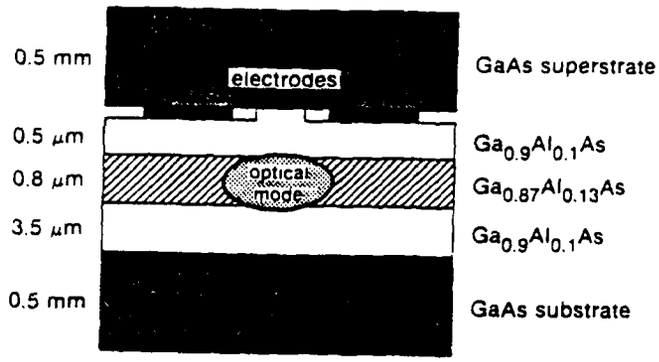

Fig. 37 >100 GHz modulator

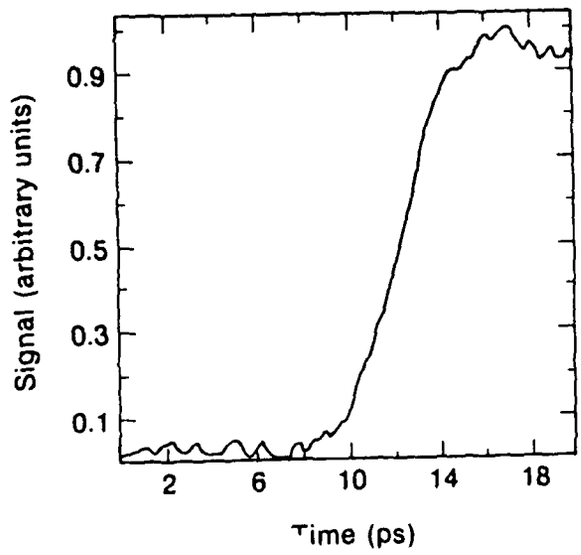

Fig. 38 >100 GHZ modulator response

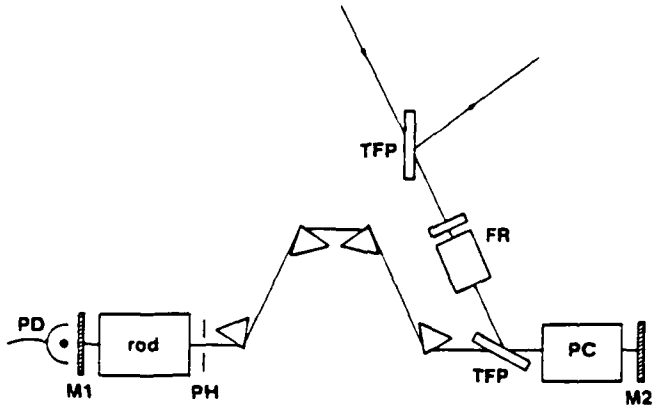

Fig. 39 Alexandrite regenerative amplifier with four Brewster prisms for cubic phase compensation. PD, photodiode; TFP's thin-film polarizers; M1, M2, high reflectors; PH, pinhole, FR, Faraday rotator and half-wave plate; PC, Pockels cell.

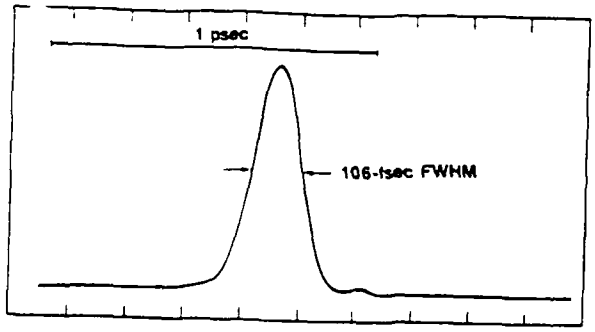

Fig. 40 Single-shot autocorrelation of the compressed pulse. The FWHM is 106 fsec, assuming a $sech^2$ pulse shape for deconvolution.